NTNU
Norwegian University of
Science and Technology

Biopolymers assisted preparation of iron based fischer-tropsch catalysts

Marit Liebe Harneshaug

Summary

Fischer- Tropsch is an alternative process to produce hydrocarbons. Hydrocarbons produced this way might replace crude oil. Iron is commonly used catalyst for FTS. This because the low cost, high availability and the low methane selectivity. A weakness of iron as catalyst for FTS is the poor mechanical stability at high temperatures. The iron particles interact with the syngas and this results in formation of iron carbides. The aim of this work is to distribute the iron particles into a solution of alginate, then characterize and test the catalysts. Alginate was produced in five different concentrations (2.5, 5.0, 10, 15 and 20 wt%). Iron nitrate ($Fe(NO_3)$ 0.1 M) were dissolved in alginate and made iron alginate beads. The iron alginate beads were washed and dried in a furnace at 80°C overnight. Large batches of 20 wt% were pyrolyzed at the conditions: 400°C 1h, 500°C 1h, 500°C 1h reproduced, 600°C 1h, 500°C 8h and 700°C 8h. The objective for this method to catalysts production is to develop catalysts with high loading of iron (40 wt%).

The catalysts samples were characterized with the instruments BET, TGA, ICP-MS, XRD, TEM and S(T)EM. The BET surface area shows the results 141, 237, 259 and $255 m^2/g$ for 2.5, 5,0, 10, 15 og 20 wt% ambient dried samples, respectively. BET surface area for the pyrolyzed samples were 22, 460, 157, 316, 298 og 393 m^2/g for 400°C 1h, 500°C 1h, 500°C 1h reproduced, 600°C 1h, 500°C 8h og 700°C 8h, respectively. TGA results shows pyrolyze range for 400-700°C. TGA results shows the iron loading 13.13, 11.83, 9.94, 7.61, 3.11 for 2.5, 5,0, 10, 15 and 20 wt% ambient dried samples, respectively. TGA results shows the iron loading 12.26, 22.81, 18.78, 24.41, 27.65 and 27.51 wt% for 400°C 1h, 500°C 1h, 500°C 1h reproduced, 600°C 1h, 500°C 8h and 700°C 8h pyrolyzed samples, respectively. ICP-MS results shows the loading of iron 12.90, 11.29, 10.64, 10.19, 6.0 for 2.5, 5,0, 10, 15 og 20 wt% ambient dried samples and 10.0, 27.40, 16.40, 28.36, 26.19 and 26.55 for 400°C 1h, 500°C 1h, 500°C 1h reproduced, 600°C 1h, 500°C 8h and 700°C 8h, respectively. In addition, the ICP-MS results shows small concentrations of sodium and sulfur in all the samples. The analysis with TEM show the most finely distribution of the particles for the catalyst 500°C 1h.

The catalysts 500°C 8h and 700°C 8h were tested in LPFT. The conversion of 500°C 8h were 5.0 % and 10.0 % at the flow ratios (H_2:CO) 1:1 and 10:1, respectively. The conversion of 700°C 8h was 8.0%. The carbon selectivity within hydrocarbon products for 500°C 8h shows highest production of C5+ for both 1:1 and 10:1. The carbon selectivity within hydrocarbon products for 700°C 8h shows highest distribution of $C_2 - C_4$ total olefins.

The catalysts 400°C 1h, 500°C 1h, 500°C 1h reproduced, 600°C 1h, 700°C 8h and the reference catalyst were tested in HPFT. 500°C 1h was a very active catalyst and was stable at the conversions 88% and 67%. 600°C 1h and 700°C 8h obtained the high conversions 86% and 92%, respectively. 600°C 1h and 700°C 8h immediately deactivated after the

highest conversions. 500°C 1h reproduced obtained the highest conversion 65%. 500°C 1h reproduced immediately deactivated to steady state range 34%. 400°C 1h had very low conversion and obtained the highest conversion 26%. The reference catalyst was steady state at 41 and 71%.

The catalysts were compared at GHSV 60 000 $cm^3/gmin$ and conversion 65%. The FTY at this comparison were $5.1 \cdot 10^{-4}$, $5.2 \cdot 10^{-4}$, $7.2 \cdot 10^{-4}$, $4.0 \cdot 10^{-4}$ and $4.4 \cdot 10^{-4}$ $molCO/g_{Fe}s$ for the catalysts 400°C 1h, 500°C 1h, 500°C 1h reproduced, 600°C 1h and 700°C 8h, respectively. The FTY for the reference catalyst was $7.9 \cdot 10^{-5} \, molCO/g_{Fe}s$. All the catalysts tested at HPFT had highest carbon selectivity within hydrocarbons of C5+. All the produced catalyst had smaller carbon selectivity of CH_4 than the reference catalysts.

Catalyst 500°C 1h had the best performance among those tested. 500°C 1h had the best particle distribution from TEM, highest BET surface area, high loading of iron and low concentrations of sodium and sulfur. The experimental work shows that the best performance are obtained in a catalyst with the following behavior: pyrolyze conditions, high iron loading, even and finely grained particle distribution and large BET surface area.

Sammendrag

Fischer-Tropsch er en alternativ prosess til petroleumsindustri for å kunne produsere hydrokarboner. Jern blir mye brukt som katalysator for Fischer Tropsch på grunn av lave kostnader, høy tilgjengelighet og lav metans elektivitet. En svakhet med jern som katalysator er at den har dårlig mekanisk stabilitet. Målet med denne oppgaven er å fordele jernpartiklene i alginatløsning og analysere om dette gir bedre mekanisk stabilitet for katalysatorene. Det ble laget jernnitratløsning $Fe(NO_3)_3$ (0.1 M) og forskjellige konsentrasjoner av alginatløsninger (2.5, 5,0, 10, 15 og 20 wt%). Alignatløsningene ble pippetert i jernnitratløsningene og dannet kuler av jernalginat. Det ble laget store mengder med 20 wt% alginatløsning. Jernalginat kulene ble vasket, tilsatt etanol og tørket i en ovn ved 80°C over natten. De store mengdene med 20 wt% alginatløsning ble pyrolysert ved forholdene: 400°C 1t, 500°C 1t, 500°C 1t reprodusert, 600°C 1t, 500°C 8t og 700°C 8t. Det var ønsket å oppnå høy konsentrasjon av jern i prøvene.

Prøvene ble karakterisert av instrumentene BET, TGA, ICP-MS, XRD, TEM og S(T)EM. BET overflate areal resultatene viste 141, 237, 271, 259 og 255 m^2/g for henholdsvis 2.5, 5,0, 10, 15 og 20 vekt% tørkede prøver. BET overflate areal for de pyrolyserte prøvene var 22, 460, 157, 316, 298 og 393 m^2/g for henholdsvis 400°C 1t, 500°C 1t, 500°C 1t reprodusert, 600°C 1t, 500°C 8t og 700°C 8t. TGA resultatene viste pyrolyseområde for 400-700°C. TGA resultatene viste jernkonsentrasjonene 13.13, 11.83, 9.94, 7.61, 3.11 for henholdsvis 2.5, 5,0, 10, 15 og 20 vekt% tørkede prøver. TGA resultatene viste også jernkonsentrasjonene 12.26, 22.81, 18.78, 24.41, 27.65 og 27.51 vekt% for henholdsvis 400°C 1t, 500°C 1t, 500°C 1t reprodusert, 600°C 1t, 500°C 8t og 700°C 8t. ICP-MS resultatene viste jernkonsentrasjonene 12.90, 11.29, 10.64, 10.19, 6.0 for 2.5, 5,0, 10, 15 og 20 vekt% tørkede prøver og 10.0, 27.40, 16.40, 28.36, 26.19 og 26.55 for henholdsvis 400°C 1t, 500°C 1t, 500°C 1t reprodusert, 600°C 1t, 500°C 8t og 700°C 8t. ICP-MS viste i tillegg små konsentrasjoner for natrium og svolvel i alle prøvene. Analysering med TEM viste finest fordeling av partiklene for katalysatoren 500°C 1t.

Katalysatorene 500°C 8t og 700°C 8t ble testet ved lavt trykk Fischer-Tropsch. Omsetningsgrad av 500°C 8t var 5.0% og 10.0% ved strøm av gass (H_2:CO) 1:1 og 10:1. Omsetningsgrad av 700°C 8t var 8.0%. 500°C 8t hadde høyest karbonselektiviteten av hydrokarboner for C5+ ved begge gass strømmene henholdsvis 1:1 og 10:1. 700°C 8t hadde høyest karbonselektivitet av hydrokarboner for $C_2 - C_4$ total olefins.

Katalysatorene 400°C 1t, 500°C 1t, 500°C 1t reprodusert, 600°C 1t, 500°C 8t, 700°C 8t og referanse katalysatoren ble testet ved høy trykk Fischer- Tropsch. 500°C 1t var en veldig aktiv katalysator og var stabil ved omsetningsgradene 88% og 67%. 600°C 1t og 700°C 8t oppnådde de høye omsetningsgradene 86% og 92%. 600°C 1t og 700°C 8t deaktiverte ummiddelbart etter høyeste omsetningsgrad. 500°C 1t reprodusert oppnådde den høyeste omsetningsgraden 65%. 500°C 1t reprodusert deaktiverte ummidelbart fram til den ble stabil ved 34%. 400°C 1t var en veldig lite aktiv katalysator. 400°C 1t oppnådde

den høyeste omsetningsgraden ved 26%. Referansekatalysatoren hadde lav omsetnings-grad og var stabil ved omsetningsgradene 41 og 71%.

Katalysatorene ble sammenlignet ved GHSV 60 000 $cm^3/gmin$ og omsetningsgrad 65%. FTY ved GHSV 60 000 og omsetningsgrad 65% var $5.1 \cdot 10^{-4}$, $5.2 \cdot 10^{-4}$, $7.2 \cdot 10^{-4}$, $4.0 \cdot 10^{-4}$ and $4.4 \cdot 10^{-4}$ $molCO/g_{Fe}s$ for 400°C 1t, 500°C 1t, 500°C 1t reprodusert, 600°C 1t og 700°C 8t. FTY for referansekatalysatoren var $7.9 \cdot 10^{-5}$ mol $CO/g_{Fe}s$. Alle katalysatorene som ble testet ved HPFT hadde høyest karbonselektivitet av hydrokarboner av C5+. Alle de produserte katalysatorene hadde mindre karbonselektivitet for CH_4 enn referanse katalysatoren.

Katalysatoren 500°C 1t var den katalysatoren som oppnådde høyest ytelse. 500°C 1t hadde best partikkel fordeling, høyest BET overflate areal, høy vektprosent av jern, lav konsentrasjon av natrium og svovel. Det eksperimentelle arbeidet har vist at høy ytelse av katalytisk aktivitet ble oppnådd fra følgende faktorer: pyrolyse, høyt BET overflate areal, høy jernkonsentrasjon og finfordelte jernpartikler.
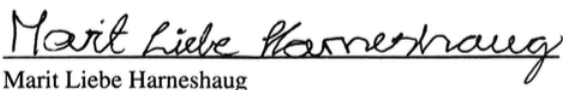
Preface

This thesis is my final work of my master degree in Chemical engineering at Norwegian University of Science and Technology (NTNU). This work is a continuation of my Specialization Project TKP4580 of Fall 2017 in Chemical Engineering. This project is given by the Catalysis Group at Department of Chemical engineering at NTNU Gløshaugen.

I would like to thank my supervisor Professor Jia Yang for guidance and discussion during the master thesis work. I would also thank my co-supervisor Professor Anders Holmen and Research Scientist from Sintef Rune Myrstad for good cooperation and enthusiasm during the execution of the master thesis work. I would also like thank Ph.D student Joakim Tafjord for your support, practical help at the laboratory and discussion around the analyzing of the results. The master work would not have been the same without you.

Finally, I would thank my boyfriend Martin Skårerverket and my family for keeping me motivated and always making me smile.

Declaration of compliance

I declare that this is an independent work according to the exam regulations at Norwegian University of Science and Technology.

Marit Liebe Harneshaug

Trondheim, Norway

June 18, 2018

Table of Contents

List of Tables

List of Figures

Abbreviations

ASF	Anderson-Schulz-Flory
BET	Brunauer-Emmett-Teller
BJH	Barret- Joyner-Halenda
EDX	Energy-Dispersive X-ray
FID	Flame Ionization Detector
FTS	Fischer-Tropsch Synthesis
FTY	Iron Time Yield
GC	Gas Chromatography
GHSV	Gas Hourly Space Velocity
GTL	Gas-To-Liquid
HPFT	High Pressure Fischer- Tropsch
HSE	Health Safety and Environment
ICP-MS	Inductively Coupled Plasma Mass Spectroscopy
IUPAC	Universally-Recognized Authority on Chemical Nomenclature and Terminology
LPFT	Low Pressure Fischer-Tropsch
MS	Mass Spectroscopy
SEM	Scanning Electron Microscopy
S(T)EM	Scannning Transmission Electron Microscopy
TCD	Thermal Conductivity Detector
TEM	Transmission Electron Microscopy
TGA	Thermal Gravimetric Analysis
WGS	Water-gas- shift
XRD	X-Rays Diffraction

Chapter 1

Introduction

1.1 Fischer-Tropsch Process

Fischer-Tropsch Synthesis (FTS) is an alternative process to produce hydrocarbons. Hydrocarbons produced this way might replace crude oil. FTS converts syngas, carbon monoxide (CO) and hydrogen (H_2), to hydrocarbons. The syngas can be produced from carbon containing feedstocks like natural gas, coal and biomass. FT process produce mainly liquid hydrocarbons, but the product can also be gas. The produced hydrocarbons can be used for fuels and chemicals.

The german scientists Franz Fischer and Hans Tropsch developed Fisher-Tropsch synthetic in 1923. The chemical reaction was described by french Paul Sabatier and Jean-Baptiste Senderens in 1902. FT process was a very important source of hydrocarbons for Germany during the Second World War. Germany had small reserves of crude oil, but large amount of coal. The coal was used to produce liquid fuels.(3) The technology at the day was high costs and ineffective and the technology could not compete with the inexpensive raw oil. (5) FTS was also an important source to produce hydrocarbons during the apartheid in South Africa.

Today, FT is an alternative attractive process because FT can use local sources of natural gas and the products can be sold in the international markets. The technology has reformed the utilization of natural gas. (5) FT process is a good alternative when the availability of crude oil is restricted or crude oil is too expensive. (6), (5) FT process is a part of the XTL process (XTL= coal-, natural gas- and biomass- to liquids). (7)

One advantage of FT technology is that are hydrocarbons produced without heavy metals pollution, sulfur or aromatic hydrocarbons. (8), (5) FT process is a special process within heterogeneous catalysis because the FTS produce different products. The conditions (temperature, pressure, metal) will determine the product distribution. (5)

Shell plant, Pearl GTL in Qatar is the largest FT plant in the world. The plant produce 140,000 barrels per day of Gas-To-Liquid (GTL) products. This plant has been in operation since 2012. Pearl GTL have been one of the most impressive new energy projects in the world.(9)

1.2   Iron as Catalyst for FTS

Iron is often used as a catalyst for the FT process because of low costs, low methane selectivity, water-gas shift (WGS) activity and wide operating temperature. (10), (11) The availability of iron is high over the world. Iron has no negative health effects.

The problem by using iron as catalyst is poor mechanical stability. The iron particles will interact with CO from the syngas and this follows to formation of different types of active iron carbides. They will not be homogeneously distributed, this result to less effective surface area. (11)

1.3   Purpose of This Work

The purpose of this work is to develop iron catalysts for FT from iron based on biopolymers. This might be a better distribution method for the iron particles. The experiment started with production of a polysaccharide gel with added iron particles into the polysaccharide gel. The type of polysaccharide used for this experiment was alginate. The objective for this method for catalysts production is to develop iron catalysis with high loading of iron (40 wt%).

For characterization of the catalysts, the instruments Brunauer-Emmett-Teller (BET), Thermal Gravimetric Analysis (TGA), X-Rays Diffraction (XRD), Inductively Coupled Plasma Mass Spectroscopy (ICP-MS), Scanning Transmission Electron Microscopy (S(T)EM) and Transmission Electron Microscopy (TEM) were used. The catalysts were tested at low and high pressure for analyzing the activity and selectivity.

Chapter 2

Theory Background

2.1 Fischer-Tropsch Process Synthesis

Fischer-Tropsch (F-T) process is a chemical reaction where syngas hydrogen (H_2) and carbon monoxide (CO) reacts to form liquids and gases of hydrocarbons. The reaction will occur on the surface of the catlysts. Commonly used metals for the catalytic surface for FT are iron, cobalt, nickel and ruthenium. (3), (12), (13) iron, nickel and cobalt are used for industrial purposes.(3), (12) The chemical reactions which will occur in the FT-synthesis when CO and H_2 react and produces to methane, olefins and paraffins, C5+ hydrocarbons and oxygenates.

The FT polymerization reactions are shown in reaction equations 2.1 and 2.2:

$$(2n + 1)H_2 + nCO \rightarrow C_nH_{(2n+2)} + nH_2O \tag{2.1}$$

$$2nH_2 + nCO \rightarrow C_nH_{2n} + nH_2O \tag{2.2}$$
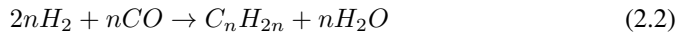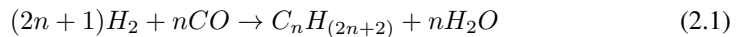
These reactions 2.1 and 2.2 are very exothermic. (12), (3)

Polymerization reactions for FTS are shown in Figure 2.1:
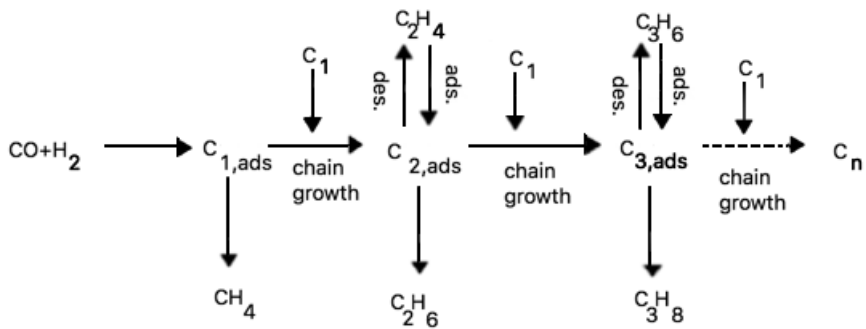
Figure 2.1: Illustration of polymerization reaction for FT. The illustration is inspired by (2).

The products from FT depends on the type of catalysts and the reaction conditions (3). Nickel-based FT catalysts have very high methane selectivity (2). The products distribution for FT will be determined from a statistical distribution developed after the Anderson-Schulz-Flory (ASF) model. The ASF model is shown in Equation 2.3.

$$W_i = i(1-\alpha)^2 \alpha^{i-1} \tag{2.3}$$

Where i is the number of carbon atoms, W_i= the weight fraction of chain length i, α= the chain growth propagation probability and $(1-\alpha)$= the probability that a chain terminates. (12) The ASF model is illustrated for the hydrocarbons in Figure 2.2:
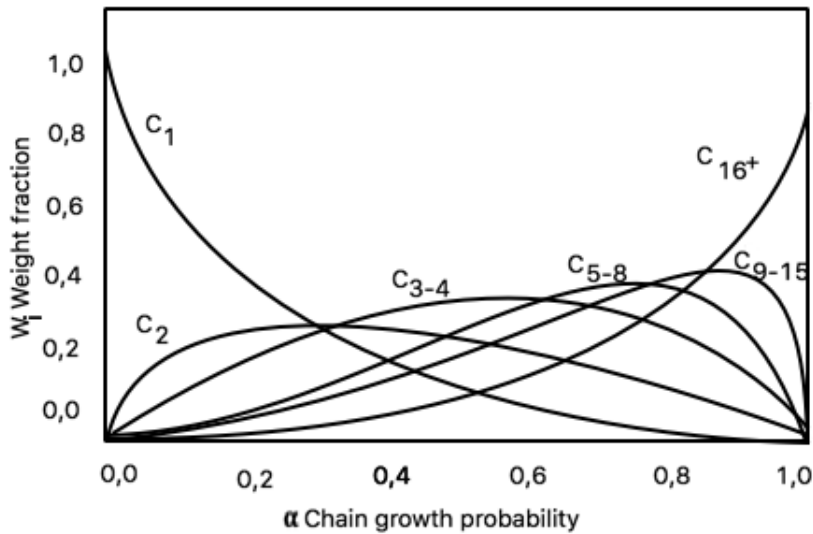
Figure 2.2: α-values for hydrocarbons produced in Fischer-Tropsch. The illustration is inspired by (3).

The chain growth probability, α for FTS are determined from the type of catalyst and process conditions. (11) Normal α-values for FT when iron at 340°C and 20 bar is used as a catalyst is 0.65-0.70 and it is shown in Figure 2.2. This produces the most C5-C8 hydrocarbons. (3), (11) The chain growth is based on reaction conditions, example ratio between H_2 and CO, changing in the pressure and temperature. (3), (2)

The principal objective for industrial FT-process is to obtain efficient exploitation, high productivity and stable operation. High selectivity of C_{5+} hydrocarbons and low selectivity of methane is best for optimizing of FT-process. (14), (15)

2.2 Iron as a Catalyst for Fischer-Tropsch

Some advantages with using iron as a catalyst is the low cost and advantageous engineering characteristics (16), (17). Iron also has high FTS- and water-gas-shift (WGS)- activity and operation conditions. (18) Iron is the preferred catalyst for FT-process when the raw material for the syngas is based on coal (CTL). This is because iron as catalyst has water-gas-shift (WGS) activity. Syngas produced from coal and biomass have a stoichiometric ratio H_2/CO lower than 2. The ratio between H_2 and CO equal to 2 is necessary for production of hydrocarbons from Equation 2.1 and 2.2. Water-gas-shift reaction is shown in Equation 2.4:

$$CO + H_2O \leftrightarrow CO_2 + H_2 \qquad (2.4)$$

Water-gas-shift is an advantage for the FT-process because it produces more H_2. Extra supply of H_2 is necessary when the raw material is made from coal. This is because the ratio between H_2 and CO is below 2. The molar ratio between H_2 and CO have to be equal to 2 according to the Equations 2.1 and 2.2. (14)

The disadvantage with iron as catalyst is poor mechanical stability. (11), (13) This is because sintering, iron phase changes, carbon deposition and follows high deactivation rates. This makes different changes for the density of the catalyst, as there is iron particle growth. (13) This results in blocking of active sites and disintegrate ion of the catalyst particles. The sintering results in loss of activity. One possible method of enhancing the mechanical properties for iron based catalyst is to disperse iron particles into a support materials. (11)

2.3 Alginates

Alginates are natural polysaccharides. Alginate consists of the monosaccharides β-D mananuric acid (M) and α-L-guluronic acid (G). The bonding between the monosaccharides are 1-4-linked. (19), (4) Alginates are produced naturally from brown algae. This type of polysaccharides are linear block-copolymers. The ratio between the M/G monomers and the length of the block polymers are dependent on the natural source (4). There are three possible irregular block wise patterns, MM, MG and GG. Carboxy groups are the main

functional groups in the block polymers. Alginate can be manufactured from alkaline extraction by treatment of $NaNO_3$, the biomass will also contain insoluble salts of calcium. It will occur cross-linking in the polymer when the amount of G-units are high. Divalent and trivalent cations are also needed for intermolecular cross-linking in the hydrogel. This gives good stability for metals which are bonded to the biopolymer. The pK_a- value for the carboxylic group will be dependent on the type of monomer. If the pH-value is below 3.5 the alginate will be precipitated. Alginate is often utilized for encapsulating metals. (20)

The blockpolymer M-M are bonded to G-G polymer are shown in Figure 2.3:

(M-M)　　　　(G-G)
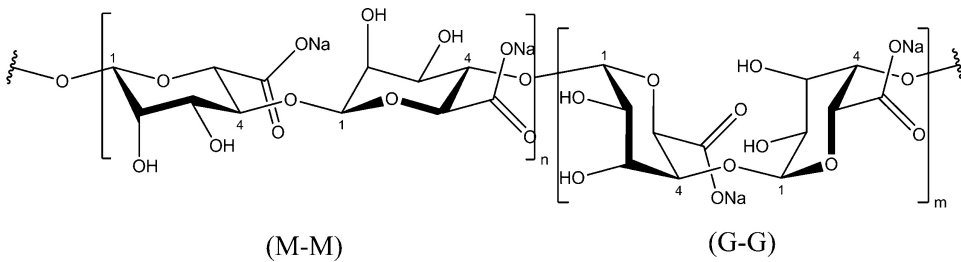
Figure 2.3: Linear biopolymer which exist of M and G- monomers. (4)

2.4   Encapsulation of Iron into Alginate

The alginate will contain long linear chains with M and G- monomers, shown from Figure 2.3. When the Na-alginate is dissolved in water, the sodium is not longer bounded to the anion groups in the alginate. Iron ions will interact with the anion chains in the alginate because iron has higher valence electron than sodium. One iron ion will interact with two anion chains from alginate. Sodium can only interact with one anion chain. The encapsulation of iron particles in to alginate is shown in Figure 2.4: (20)
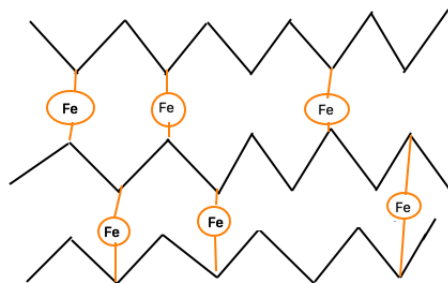
Figure 2.4: Encapsulation of iron particles into alginate polymer.

If the encapsulated metal algiante is pyrolyzed, only the carbon and the metal will remain.

2.5   Washing Prior to Drying

The encapsulation of iron ions in to an alginate polymer will compose a hydrogel. Hydrogels have poor durability during ambient drying due to the high surface tension of water, which will make the gel structure collapse. A alcogel will conserve the iron alginate better. To acchive optimal alcogel it is best to add ethanol gradually. This will also make it easier to remove superficial particles of iron. One method for drying the iron alginate is in a furnace at 80°C. (20)

2.6   Instruments

The instruments, analyzing methods and techniques are described in this chapter. For characterization of the samples it was necessary to analyze the pore structure and surface area, temperature degradation, pyrolyzation temperature, structure in electron microscope.

2.6.1 Brunauer Emmett and Teller (BET)

Brunauer, Emmett and Teller (BET) is a physical technique to calculate the surface area of a material. The method can also determine the pore structure and pore radius for a material. BET method can be used for porous material with a surface area larger than 1 m^2/g. The method is based on adsorption of a gas (N_2) at liquid N_2 temperature (77 K) onto an internal surface of the carrier. One adsorbed N_2 molecule will occupy an area on the surface equal to a cross-sectional area for a N_2 molecule. This cross-sectional area is $16.2 \mathring{A}^2$. The measuring of the adsorption isotherm the absorbent will be held at a constant temperature. This constant temperature has to be near the boiling point of the adsorptive. (21)
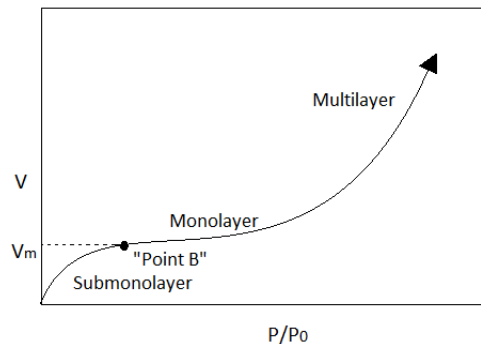
Figure 2.5: Schematic illustration of a BET isotherm. The illustration is inspired by (3).
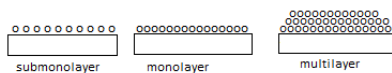
Figure 2.6: Illustrated three types of layers for BET isotherm. The illustration is inspired by (3).

Schematic illustration of BET isotherm is prepared and shown in Figure 2.5. The relative pressure (P/P_0) is plotted by quantity adsorbed (cm^3/g). To the left of the graph the adsorption will occur like a submonolayer. The submonolayer is when an amount of gas molecules adsorbs to the surface. The distance between the molecules on the surface is different. There is space for more molecules on the surface. The flat part on the graph after the boiling point in the graph is the monolayer. In the monolayer all the active sites on the catalyst surface will be filled. The second rise is multilayer, here gas molecules will adsorb to each other in layers. The three types of layers are illustrated in Figure 2.6.
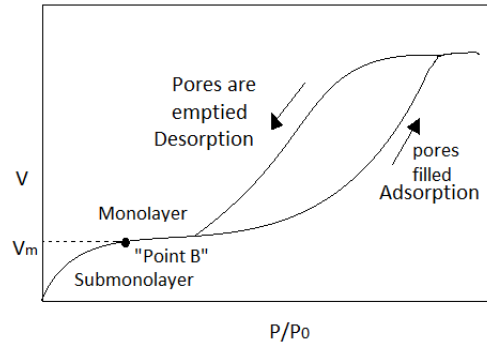
Figure 2.7: BET isotherm, shows adsorption and desorption areas. The illustration is inspired by (3).

The surface area of the particles can be calculated from the adsorption isotherm equation. The BET equation describes the relationship between the volume of adsorbed gas (N_2) at a given partial pressure and the volume adsorbed gas at a monolayer coverage. The BET adsorption isotherm equation is given by BET equation (2.5):

$$\frac{P}{V(P_0 - P)} = \frac{1}{V_m C} + \frac{(C-1)P}{V_m C P_0} \qquad (2.5)$$

P= partial vapour pressure of adsorbate gas, N_2
P_0= saturated pressure of adsorbate gas at the experimental temperature
V= volume adsorbed gas at pressure P
V_m= volume adsorbed gas at a monolayer coverage
C= a constant
(22), (3), (23)

The BJH-method (Barrett-Joyner-Halenda-method) is available to estimate the volume of the pore structure. The BJH method is based on the theory that the pores will be filled with nitrogen. At high relative pressure, N_2 will condense in the catalyst pores. The pore volume and the pore size can be estimated from Kelvin Equation 2.6:

$$ln(\frac{P}{P_0}) = -\frac{2\sigma V cos\Theta}{rRT} \qquad (2.6)$$

σ= surface tension of liquid nitrogen
Θ=contact angle
V= molar volume of liquid nitrogen
r = radius of the pore
R = gas constant
T= absolute temperature
P= measured pressure
P_0= saturation pressure

There are three classifications of porosity. If the pore width (diameter) is below 2 nm, this type of pore is classified as a micropore. If the width is between 2 and 50 nm, this type of pore is a mesopore. If the pore width is larger than 50 nm the pore is a macropore. (3)

IUPAC have classified four different adsorption-desoprtion hysteresis. The four hysteries is shown in Figure 2.8:
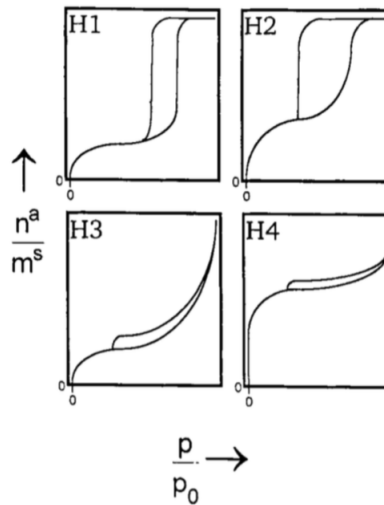
Figure 2.8: Four different adsorption-desoprtion hystereses (3).

The H1 and H2 characterize two different mesopore structures. H1 describe an adsorbent with a distribution of uniform mesopores. H2 has a more complicated network. The hysteresis H3 and H4 does not have a limit for the adsorption of high pressures (3).

BET is somewhat an inexact technique because the technique is based on several assumptions. This is the limitations of BET technique. The BET isotherm will provide the assumptions:

- It will adjust a dynamic equilibrium between the adsorbate and the adsorptive.

- The rate of adsorption and desorption inn all the layers will be equal.

- In the first layer, monolayer, one molecule will only adsorb to one active site.

- The adsorbed molecules in the first layer compose the adsorption sites for molecules in the next layer.

- The interactions between the adsorbates are ignored. The conditions for adsorption and desporption are the same for all the layers.

- The adsorption energy for molecules who are in second or higher layers will be like the condensation energy.

- If the saturation pressure is equal to the partial vapor pressure of adsorbate ($P=P_0$) the multilayer will grow to infinite thickness.

The samples were analyzed with BET for determination of surface area, pore volume and average pore diameter of the catalysts. BET isotherm was used for calculation of surface area and BJH method was used for calculation of pore volume and average pore diameter.

2.6.2   Thermal Gravimetric Analysis (TGA)

Thermal Gravimetric Analysis (TGA) is used to study the thermal characteristics. The technique which the mass of the sample shows the thermal response as a function of temperature. (24) The method can be used for analyzing adsorption, dehydration, evaporation, sublimation and chemical reactions. (25) The technique will also give information about the thermal degradation of the biomass. The data will give information about degradation mechanisms and the kinetic models. (24)

Some TGA instruments have a connected mass spectroscopy (MS). The MS will detect the flue gas (H_2O, CO_2, CO, CH_4, NO_2, NO etc.) from the sample. The flue gas will occur while the sample is degraded as function of temperature. (26)

The samples will be destroyed after the TGA analysis, but the sample can be used for further XRD analysis. TGA was used to analyze the temperature reaction area and the MS were used to calculate the loading of iron.

2.6.3   Inductively Coupled Plasma Mass Spectroscopy (ICP-MS)

Inductively Coupled Plasma Mass Spectroscopy (ICP-MS) is a very accurate quantitative analyze method to determine the content of the elements. The method is based on measuring the characteristic emission from electromagnetic radiation. The instrument can analyze the following elements: Fe, Na, Li, Be, B, Al, V, Cr, Mn, Co, Ni, Cu, Zn, Ga, Ge, As, Se, Rb, Sr, Mo, Pd, Ag, Cd, Sn, Sb, Te, Ba, W, Pt, Hg, Ti, Pb, Bi and U. The samples have to be diluted in purified water and dissolved in HNO_3. (27)

Plasma is an electrical neutral gas consisting of positive ions and free electrons. The plasma has adequately high energy to atomize, ionize and excite most of the element. The plasma consists of argon, helium, nitrogen and air. The temperature for the plasma is 6000-8000°C. ICP is availed for ionizing sources for the analyzing technique ICP-MS. ICP-MS is mass spectroscopy to separate and detect the ions produced in the plasma. (28)

A solution of a sample will be pumped in to the plasma with an atomizer, this will make an aerosol of the sample. The aerosols will be transported during the plasma. The aerosols will atomize and ionize because of the very high temperature. Small amount of the atoms and ions will be exited and give the characteristics electromagnetic radiation, then they will emit back to standard. (29)

ICP-MS was used to determine the concentration of the different elements in the samples.

2.6.4   X-Ray Diffraction (XRD)

X-ray diffraction (XRD) is a technique identifies crystalline phases inside in samples by lattice structural parameters. The technique can determine the particle size. The technique is qualitative analyzing method. (3)X-ray diffractometers consists of three elements, a X-ray tube, a sample holder and a detector for x-rays. (30)

X-ray diffraction arises in the elastic scattering of photons from X-ray by atoms in a periodic lattice. The scattered monochromatic X-rays as are in the phase will give constructive interference. (3), (30) The x-rays will be produced from a cathode ray tube. Further the x-rays will be filtered to generate monochromatic radiation. The beam also will be concentrated and coursed into the sample. The sample and the direction for incident rays gives constructive interference and diffracted ray. This is because of Braggs law, (Equation 2.7). (30)

$$n\lambda = 2dsin\Theta \qquad (2.7)$$

λ = wavelength of the X-rays
d = Distance between two lattice planes
Θ = angle between the normal to the reflecting lattice plane and the incoming X-rays
n = the order of reflection (an integer) n=1,2,3...
(3), (30)

Braggs law applies for the wavelength of electromagnetic radiation to the diffraction angle and the lattice spacing. This connection is only for crystalline samples. Further in the XRD characterization the x-rays will be detected by a detector. It is possible to analyze the sample in a range of 2Θ angles, this gives all feasible diffraction direction of the lattice. Analyzing in range of 2Θ angles is best when the sample is a powdered material. For powdered material, data can be collected between 5 and 70 ° angles. (30)
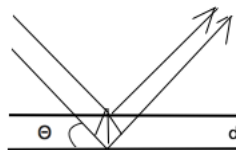
Figure 2.9: Braggs law. The illustration is inspired by (3).
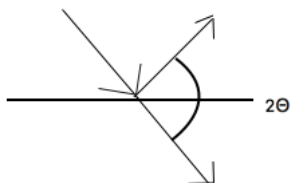
Figure 2.10: 2Θ. The illustration is inspired by (3).

Scherrer equation estimate the crystal size:

$$< L >= \frac{K\lambda}{\beta cos\Theta} \tag{2.8}$$

$< L >$ = A measure of the dimension of the particle in the direction perpendicular to the reflecting plane
λ= Wavelength of X-ray
β= Peak width
Θ= Angle between the beam and the normal to the reflecting plane
K= constant, often equal to 1

XRD was used to determine the phase composition of the catalysts. The literature show carbon materials are amorphous (31). Therefore they can not be characterized with XRD.

2.6.5 Electron Microscopy

Electron microscopy is a technique for imaging samples who are too small to be analyzed by a normal light microscope. The electron microscope use beams of electrons. The beam has smaller wavelengths than visible light. Electron microscopy can give information about the surface behaviour crystallography, morphology and chemical composition. (32)

Transmission Electron Microscopy (TEM)

Transmission electron microscopes (TEM) analyze the inner structure of the sample, this give two-dimensional pictures (3). TEM have a beam of electrons who passes through a very thin and carefully prepared sample. This electron beam is focused at a screen for characterizing the structure of the sample. (32)

TEM instrument consist of an electron gun, electromagnetic condenser spindle, electromagnetic lens, fluorescence screen and the sample. First the electron gun will send out a beam of electrons. The purpose of the electron beam is to send electrical current between a wolfram filament. This gives higher acceleration of the electron beam. The voltage will accelerate from 80-200kV and end up at 1 MV. Further the electron beam will pass the electromagnetic condenser spindle, this will focus the electron beam. The sample will be irradiated through the focused electron beam. At the fluorescence screen the energy of the electrons will be converted to visible light. This will occur because the wavelength of the electrons will be extended. This gives a picture of the structure of the sample. (33)

The limitation and requirement for the sample when analyzing with electron microscopy is that the samples have to be dried material, solid and stable for low pressures. The sample have to withstand the heating from the electron beam. If the sample has very a heterogeneous structure the results will give little representation of whole the sample. Anyway, TEM can give valuable results of small areas in the sample. (34) TEM-sample has to be thin enough to enable transmission of sufficient amount of electrons to form a picture by minimum energy loss. (33)

Scanning Electron Microscopy (SEM)

Scanning electron microscopy (SEM) analyze the surface behaviour composition and topology of the sample. Samples for SEM is often coated with gold or carbon on the surface. This to improve the results of the analysis.

The SEM instrument consist of an electron gun, condenser lenses, scan coils, objective lens, sample and the two detectors, X-ray detector and electron detector. The electron gun sends out a beam of electrons. The electron beam will be focused by the condenser lenses. The scan coils focus the beam to very small beam. The width of the beam increase into the objective lens. After the objective lens the beam meet the sample. The electron beam excites primer electrons. When primer electrons meet the sample, they will reflect out secondary electrons, also called backscattered electrons and x-rays. Backscattered electrons have low energy. The backscattered electrons and the x-rays will be detected by the electron and x-rays detector. The detectors will give images for the structure of the sample. (3)

Scanning Transmission Electron Microscopy (S(T)EM)

Scanning transmission electron microscopy (S(T)EM) is an electron microscopy with combined both TEM and SEM modes. The scanning coils will be used to light up small areas in the sample to obtain light and dark-field pictures.

The primary beam can be like TEM if the beam is generated with a field emission gun. For analyzing samples of metal, it can be difficult to see the metal particles. One solution is to increase the contrast of the picture, this can be used with dark-field modes. Dark-field modes will give pictures of electrons which diffracted the metal particles. For analyzing with annular dark-field the sample have to be placed on a grid.

Energy-Dispersive X-rays (EDX) is a detector for analyzing the elements in the sample. In the SEM instruments x-rays will be bi-products from the electron microscopy. The x-rays will be detected from a x-ray detector. The detected signals will describe the elements which are present in the sample. The EDX will also give information of the amount of each element in the sample. (3)

The set-up for the three different types of electron microscope are shown in Figure 2.11:
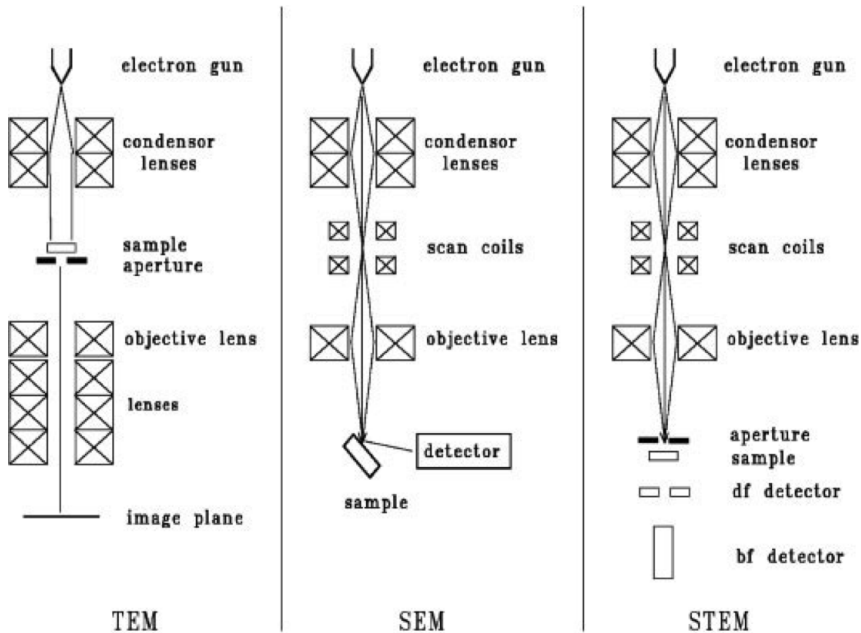
Figure 2.11: Illustrated set-up for the three different types of electron microscope, TEM, SEM and S(T)EM. (3)

2.7 Catalyst Testing

It is necessary to determine the activity and the selectivity of the catalyst. The activity and selectivity can be tested both at low and high pressure. The catalysts can be activated by reduction in a reduction medium. For Fischer- Tropsch experiments a mixture of hydrogen and helium are often used during the reduction and low pressure.

CO Conversion (X_{CO}) will quantify the amount of converted CO. Definition of conversion is shown in Equation 2.9: (35)

$$X_{CO} = \frac{\text{Moles of CO reacted}}{\text{Moles of CO fed}} \qquad (2.9)$$

The catalysts testing will give the following products: CO_2, CH_4, $C_2 - C_4$ total olefins, $C_2 - C_4$ total parafin and C5+. The reaction feed and the achieved products can be analyzed and quantified by a gas chromatography (GC). (36)

2.7.1 Low Pressure Fischer-Tropsch (LPFT)

In the low pressure Fischer-Tropsch test the catalysts activity and selectivity will be tested at low pressure 1 bar and 340°C.

2.7.2 High Pressure Fischer- Tropsch (HPFT)

In the high pressure Fischer-Tropsch test the catalysts activity and selectivity will be tested at high pressure 20 bar and the high temperature 340°C. CO conversion for HPFT will be calculated from 2.10:

$$X_{CO}(\%) = \frac{F_{CO(in)} - F_{CO(out)}}{F_{CO(in)}} \cdot 100 \qquad (2.10)$$

The inlet composition of the syngas for FT are N_2:CO:H_2 (3: 48,5 :48,5 mole %). N_2 is inert gas so the inlet composition of the syngas and the outlet composition of the products are always 3 mole %. The inlet composition of CO is 48,5 mol% and the outlet composition of CO will be determined from Equation 2.11:

$$\frac{A_{CO,t=0}}{A_{N_2,t=0}} = \frac{A_{CO,t=1}}{A_{N_2,t=1}} \qquad (2.11)$$

Gas hourly space velocity (GHSV) is a measure of reactant gas flow rate per reactor volume. The definition for GHSV is shown in Equation 2.12 and the unit for GHSV is [cm^3/g min].

$$GHSV = \frac{\text{volume of syngas (mL)}}{g_{catalyst} \cdot \text{hour}} \qquad (2.12)$$

Iron time yield (FTY) is initial catalytic activities. FTY is a measure of mole of CO

converted to hydrocarbon per time (s) per weight of iron (g). FTY has the unit [mole/g_{fe} · s] (13) FTY is given by Equation 2.13:

$$FTY = X_{CO} \cdot F_{CO} \left(\frac{1 - S_{CO_2}}{V_m \cdot 60 \cdot m_{cat} \cdot \frac{X_m}{100}} \right) \tag{2.13}$$

X_{CO} = conversion of CO [%]
F_{CO} = Flow of CO [mL/min]
S_{CO_2} = Selectivity of CO_2 at the given CO conversion [%]
V_m = Molar volume [L/mole]
X_m = Fraction of metal in the catalyst [%]
$m_{catalyst}$ = mass of metal in the catalyst [g]
(13)

Experimental Methods

The following subchapters give detailed description about the method for the experimental work. The chapter is introduced with preparation of the catalysts. Then the chapter give description about the characterization of the catalysts and the testing of the catalysts.

3.1 HSE Risk Evaluation

Prior to start of the experimental work at the laboratories, a HSE risk evaluation of the experiment was carried out. Procedure for the instruments at the laboratory were discussed. The hazard elements were noted and the efforts for them were considered. The risk evaluation is shown in Appendix A. Laboratory work could not commence before the HSE risk evaluation and necessary precautions was established.

3.2 Catalyst Preparation

A solution of iron-nitrate, $Fe(NO_3)_3$ (0.1 M) was prepared in a volumetric flask (500 mL). It was weight out mass of $Fe(NO_3)_3 \cdot 9\ H_2O$ (20.19 g). Deionized water was used to dissolve the salt.

Solutions of alginate was made in the concentrations 2.5, 5.0, 10.0, 15.0 and 20 wt%. The type of alginate was LFR5/60 S21799. The alginate was dissolved in deionized water by a magnetic stirrer. When the alginate was dissolved, the alginate was pipetted into the iron-nitrate solutions (50 mL) and this made the iron-alginate-beads. Overview for concentrations for the solutions are shown in Table 3.1:

Table 3.1: Overview for concentrations for alginate solutions for production of catalysts.

wt%	2.5	5.0	10.0	15.0	20.0
weight of alginate [g]	0.25	0.50	1.00	1.50	2.00
volume of deionized water [mL]	9.75	9.5	9.0	8.5	8.0

Larger batches of 20 wt% alginate was also made. Alginate (10 g) was weight out and dissolved parts by parts in deionized water (40 mL). A magnetic stirrer was used. The calculations for iron -nitrate $Fe(NO_3)_3$ solution and the different calculations for alginate solutions are shown in Appendix B.

3.2.1 Washing Prior to Drying

The set up for the washing procedure is shown in Figure 3.1. Suction flask with a Buchner funnel filter, type of filter, ME24/21ST 0.2 μm was used. The alginate was washed by deionized water (200 mL) 4 times. Thereafter, the volume of iron alginate beads was filled up with deionized water.
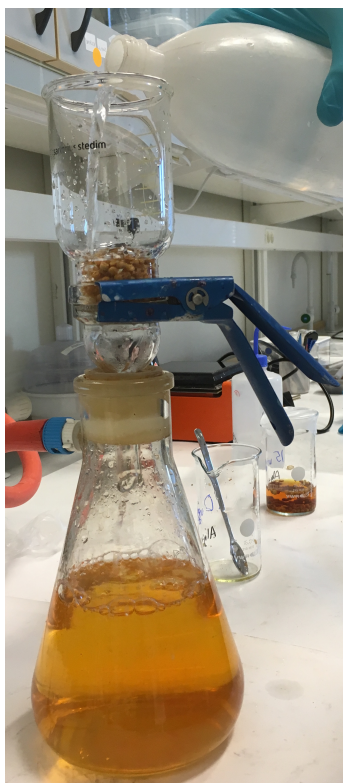
Figure 3.1: Washing of iron alginate beads by deionized water.

After waiting for 15 minutes, deionized water was removed and the ethanol concentrations were increased gradually. This to not destroy the pore structure of the alginate. The iron alginate beads was added solutions of ethanol-water in five different concentrations (15, 35, 55, 75 and 100 % of ethanol). The different concentrations were filled up and taken away by intervals of 15 minutes. The work started with the lowest concentration of ethanol.

The alginate solution was placed in ethanol for 24 hours before drying. The purpose of the washing was to remove unbounded iron and sodium ions. It was necessary to wash iron alginate beads with ethanol prior to drying because ethanol keep the pore structure better than water.

3.2.2   Drying

For drying the samples were placed in to a furnace at 80°C during the night. Then the iron-algiante beads were crushed with a mortar and pestle to get a homogeneous iron alginate sample.

3.2.3   Pyrolyze

The large batches of iron alginate samples (20 wt%) were pyrolyzed. Amounts of samples were weight out (20 wt%, 6 g) and placed in to a calcination reactor of glass. The reactor was placed in a tubular oven, shown in Figure 3.2a. N_2 gas (100 mL/min) was passed through the reactor. It was pyrolyzed in the temperature range 400-700°C. The iron alginate samples were pyrolyzed at the different temperatures 400°C, 500°C and 600°C for 1 hour. The heating rate was 5°C/min. In addtion, two samples were pyrolyzed for 500°C and 700°C for 8 hours. The heating rate was 2°C/min. All the samples were cooled to room temperature and passivated for 60 minutes with Helium/O_2 atmosphere (100 mL/min, 1% O_2 in Helium). The reactor of glass and pyrolyzed sample is shown in Figure 3.2b. Then, the samples were crushed by mortar and pestle.

(a) Calsination reactor in the tubular oven.
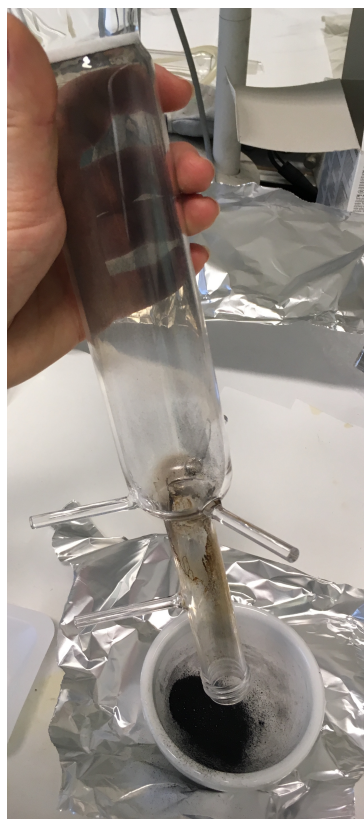
(b) Calsination reactor and a pyrolyzed sample.

Figure 3.2: Calsination reactor.

3.3 Characterization of the Catalysts

3.3.1 BET

Tristar 3000 surface area and porosity analyzer was used for measurement and Micrometeritics VacPrep 061 Sample degas system was used for degasing. The amounts of samples (10-50 mg) were weight out. Both ambient dried samples and pyrolyzed samples was analyzed with BET. The tubes were weight before and after adding of samples, the weights were noted.

The samples were degassed during the night at 80°C and evacuated at 200 mTorr. The tubes were also weight after the degassing. The analysis of samples 20 wt % pyrolyzed 400°C 1h and 20 wt % pyrolyzed 500°C 1h reproduced were repeated. In addition, the samples 20 wt% pyrolyzed 400°C 1h and 20 wt% pyrolyzed 500°C 1h reproduced were

also analyzed with 200°C as degas temperature. Degas temperature 200°C was tested because this can give higher BET results than 80°C. Pyrolyzed samples tolerate higher temperatures than 80°C.

3.3.2 TGA

Two different types of measurements were performed- dried samples in argon to mimic the pyroysis conditions and both ambient tried and pyrolyzed samples in air in order to calculate the weight loading of iron. NETZSCH STA 449 was used for measuring the temperature reaction range and the NETZSCH QMS 403 was measured the MS. A calibration file was created for these two atmospheres in order to have a benchmark for the measurement. This was performed by subjecting an empty sample holder to the conditions it would undergo. The results for this empty sample holder was substracted for the sample measurements.One calibration file for argon were made and one for air.

The temperature program for TGA was 25 to 900°C with temperature heating rate 10°C/min. The flow of gas was 75 mL/min. The samples were weight out (10-30 mg) and noted. Procedure for the instrument was followed. The samples were placed in the instrument and flushed with argon for 1 hour. After flushing with argon, the measurement recording started. It was important to remove other gases before the measurement started. The samples analyzed in air it was not necessary with flushing. The procedure for TGA was followed.

3.3.3 ICP-MS

The ambient dried samples in the different concentrations (2.5, 5.0 , 10, 15 and 20%), pure alginate and the pyrolyzed samples (400°C 1h, 500°C 1h, 500°C 1h reproduced, 500°C 8h, 600°C 1h, 700°C 8h) were analyzed with ICP-MS.

The procedure for the ICP-MS was started with washing the UltraClave tubes in water. The amounts of samples (50-70 mg) were weight out. 3 blank samples were also used. . The samples were added HNO_3 (50% vol 6 ml). The autoclave tubes were set in the UltraClave with a special temperature program. The temperature profile is shown in Appendix D. The temperature was increased from 20 to 220 °C in the temperature program.

Then the samples were diluted in purified water to the concentration of HNO_3 was 0.6 M. The samples were filled in special tubes for ICP-MS and analyzed with the ICP-MS instrument.

3.3.4 XRD

All the pyrolyzed samples were characterized with XRD. In preparation for XRD characterization, the samples were put in to dedicated XRD sample holders. Procedure for instrument Da Vinci 1 Diffraction was followed. The angle for the monochromatic beam was 20-80° 2Θ V6 at 30 minutes.

3.3.5 S(T)EM

Hitachi S-5500 S(T)EM was used to determine the size and the compositions for the particles. The detector XFlash EDX Detector were used. Pyrolyzed samples were analyzed by S(T)EM. A special plate for S(T)EM was added ethanol and a very small amount of sample was put on the surface of the plate. The preparation for S(T)EM is shown in Figure 3.3.
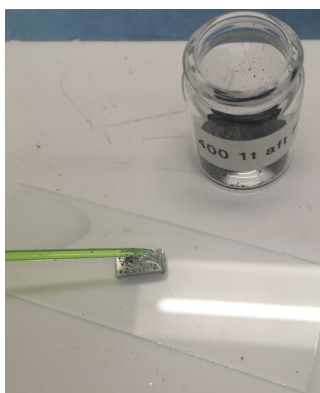
Figure 3.3: Preparation for S(T)EM.

3.4   Catalyst Testing

3.4.1   Low Pressure Fischer-Tropsch (LPFT) Test

The samples and silicon carbide were sieved at the fraction 90-250 μm. The amounts of samples (50 mg) and silicon carbide (200 mg) were weight out and mixed. A U-reactor made of quartz was used. Quartz wool was put in to the U-reactor and compressed for insulation purpose. The mix of catalyst and silicon carbide was also put in the reactor. Quartz wool was put in the U-reactor over the mix. The reactor was mounted in the low-pressure-FT-rig, and the thermocouple was fixed in the U-reactor (shown in Figure 3.4).

Figure 3.4: U-reactor for LPFT test.

The flow was set to H_2 (20 mL/min) and Ar (30 mL/min). The low-pressure-FT-rig was checked for leakage. After the leak test was completed the furnace was lifted over the reactor by a wire. The top of the furnace was insulated with quarts wool.

The temperature program for the reduction reaction was started to increase the temperature 5°C/min to 350°C with the flow H_2 (20 mL/min) and Ar (30 mL/min). This temperature was kept for 2 hours. Then the temperature was cooled to 340°C, with a temperature rate at 2°C/min. When the temperature was cooled to 340°C, the syngas (H_2=1.5mL/min, CO=15mL/min, Ar=33.5 mL/min) was added. Further the temperature was kept at 340°C for 20 hours. Temperature program for Low-pressure test is shown in Figure 3.5. The pressure was measured.
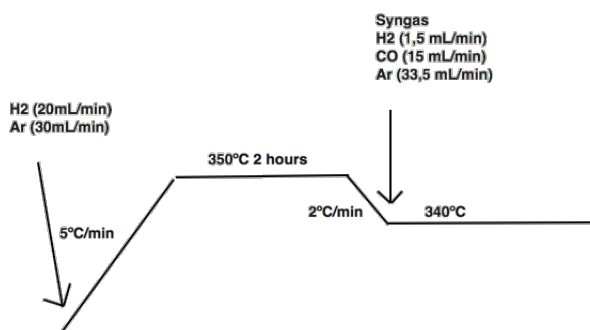
Figure 3.5: Temperature program for Low pressure FT test.

Feed Analyze

The feed was analyzed with a GC. The feed was analyzed in the flow ratios H_2:CO 1:1 and 10:1. 3 measurements was taken per ratio. For the flow ratio 1:1 the composite for the flow was H_2:CO:Ar 1.5:1.5:47 (mL/min). For the flow ratio 10:1 the composite for the flow was H_2:CO:Ar 15:1.5:33.5 (mL/min).

3.4.2 High Pressure Fischer-Tropsch (HPFT) Test

The samples and silicon carbide were sieved at the fraction 90-250 μm. The amounts of catalyst (250 mg) and silicon carbide (6.75 g) were weight out and mixed. The metal cylinder with grid was put in the fixed-bed reactor. Quartz wool was put in reactor and compressed for insulation purpose The sample was put in the fixed-bed reactor and then filled with more quartz wool. The fixed-bed reactor was mounted in the High Pressure FT shown in Figure 3.6. The system was leak tested with helium. After the leak test was completed, the pressure valves downstream the reactor were opened.

Figure 3.6: The reactor fasten in the HPFT-rig.

The type of GC used for the experiment was 6890N Network GC System from Agilent Technologies. The system was connected to FID and TCD. One measurement per hour was made with the GC.

The temperature program for the reduction reaction was started. The temperature was increased at a rate of 5°C/min up to 350°C. The pressure was 3 bar, H_2 flow was 40 mL/min and He flow was 80 mL/min. Thereafter, the temperature was reduced to 280°C with a heating rate of 2°C/min. Further the temperature was increased from 280°C to 340°C with a temperature heating rate of 2°C/min. The temperature program for FT is shown in Figure 3.7:
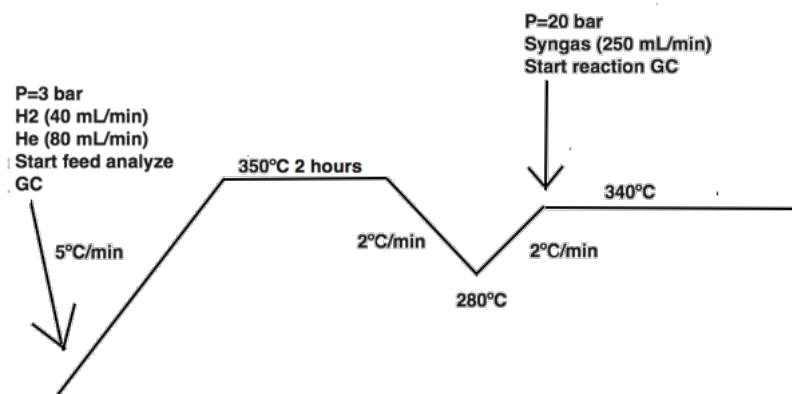
Figure 3.7: Temperature program for High pressure FT test.

Feed Analyze

The feed was analyzed during the reduction reaction.

Reaction Analyze

When the temperature was 340°C, the pressure was 20 bar and the syngas was introduced (250 mL/min, H_2:CO 1:1) the measuring was started. After completion of the test, the system was flushed with helium. The 20 %wt pyrolyzed samples 400°C 1h, 500°C 1h, 500°C 1h reproduced, 600°C 1h and 700°C 8h were tested at the High pressure FT. A reference catalysts Amax from Clariant (37) was also tested at the High pressure FT. This catalyst is an industrial HTFT catalyst for Fischer Tropsch. The loading of iron is 92.0 %wt. The 20 %wt pyrolyzed samples were compared with the reference catalysts.

After the FT-testing the samples were analyzed with TEM. The silicon carbide was removed during sieving.

Analyzing with TEM of FT-samples

The analysis with TEM was executed at a laboratory in China organized by Professor Jia Yang at NTNU (38). The same procedure for preparation for TEM was executed for S(T)EM described in Chapter 3.3.5. The particles size in the TEM pictures were calculated from the program Image processing and Analysis in Java, ImageJ.

Chapter 4

Results

This chapter presents the results from production of catalysts, characterization from the instruments and the testing of the selectivity and activity. The results will be commented and discussed in Chapter 5.

4.1 Catalyst Preparation

The different concentrations of alginate solutions gave different characteristics. The lowest concentration of alginate solution was easiest to dissolve. It was difficult to dissolve those with the highest alginate concentration. When ethanol-water was added in to the alginate solutions one could see small bubbles from the alginate rise up to the surface of the solution.
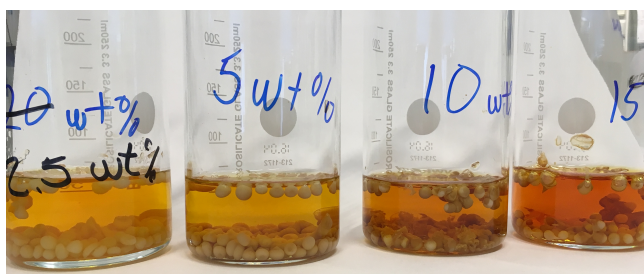
Figure 4.1: Shows the four concentrations of iron-nitrate solutions. The concentrations is increasing from left to the right.

The Figure 4.1 shows the different iron-alginate solutions. The colour for the solutions is darker for those with higher concentration. Description for the consistency for the different concentrations of iron alginate beads are shown in Table 4.1:

Table 4.1: Description for the consistency for the different concentrations of iron alginate beads.

Concentration [wt%]	Comments of the consistency for the iron alginate beads
2.5	Like shells
5.0	Slightly hollow spheres some with tails
10	Deform clumped together
15	Difficult to dissolve
20	Very difficult to dissolve

4.2 Characterization of the Catalysts

4.2.1 BET

Ambient dried and pyrolyzed samples were analyzed with BET. Isotherm linear plot for 5% ambient dried sample is shown in Figure 4.2:
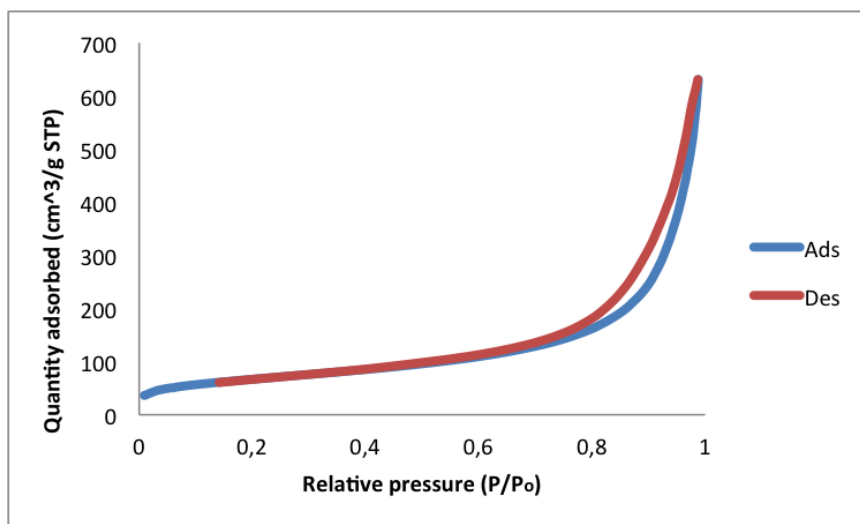
Figure 4.2: Isotherm linear plot for 5.0% ambient dried sample, blue line = adsorption and red line= desorption (Degas temperature 80°C).

The isotherm linear plot for 5% ambient dried is like a H3-hysteresis, shown from Figure 4.2. Described in Chapter 2.6.1 IUPAC have classified four different adsorption- desorption hysteresis for BET. The BET isotherms for all the ambient dried samples had equal hysteresis for all the ambient dried samples.

BET surface area for ambient dried samples are shown in Figure 4.3:
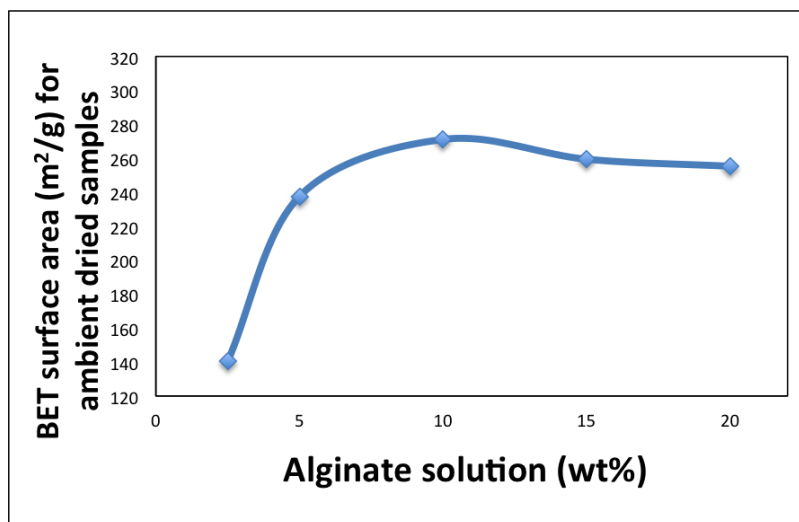
Figure 4.3: BET surface area for ambient dried samples (Degas temperature 80°C).

The sample 2.5 wt% ambient dried has the smallest BET surface area (141 m^2/g) of all the ambient dried samples, this is shown in Figure 4.3. The surface area for 5.0 wt% ambient dried is much larger than the BET surface area (238 m^2/g) for 2.5 wt% ambient dried. 10 wt% ambient dried has the largest BET surface area (271 m^2/g) of all the ambient dried samples. The BET surface area for 15 wt% and 20 wt% ambient dried have the surface area 259 m^2/g and 255 m^2/g, respectively. 10 wt% ambient dried has the maximum BET surface area.

Pore volume and pore size for ambient dried samples are shown in Table 4.2:

Table 4.2: Pore volume and pore size for ambient dried samples (Degas temperature 80°C).

Sample	BET surface area [m^2/g]	Pore volume [cm^3/g]	Pore size [nm]
2.5 wt% Ambient dried	141	0.64	16.9
5.0 wt% Ambient dried	237	0.99	16.0
10 wt% Ambient dried	271 ± 33	1.17 ±0.02	15.5 ±0.7
15 wt% Ambient dried	259	1.02	14.6
20 wt% Ambient dried	255	1.05	15.0

The pore volume for the ambient dried samples increase by larger BET surface area, shown from Table 4.2. The pore volume for ambient dried samples decrease for smaller BET surface area. There is small difference between the pore sizes for all the ambient dried samples because all the ambient dried samples have pore size range 14.6-16.9 nm.

BET surface area, pore volume and pore size for pyrolyzed samples are shown in Table 4.3:

Table 4.3: BET surface area, pore volume and pore size for pyrolyzed samples (Degas temperature 80°C and 200°C).

Sample	BET surface area $[m^2/g]$	Pore volume $[cm^3/g]$	Pore size [nm]
20 wt% Pyrolyzed 400°C 1h (d=80°C)	22.2 ± 0.8	0.10	18.2 ±0.6
20 wt% Pyrolyzed 500°C 1h (d=80°C)	460	0.96	13.0
20 wt% Pyrolyzed 500°C 1h reproduced (d=80°C)	157 ±1	0.28	13.8
20 wt% Pyrolyzed 600°C 1h (d=80°C)	316	0.58	13.7
20 wt% Pyrolyzed 500 °C 8h (d=80°C)	298	0.59	13.0
20 wt% Pyrolyzed 700 °C 8h (d=80°C)	393	0.57	12.2
20 wt% Pyrolyzed 400°C 1h (d= 200°C)	24.4	0.10	19.3
20 wt% Pyrolyzed 500°C 1h reproduced (d=200°C)	199	0.30	14.7

Catalyst 20 wt% Pyrolyzed 500°C 1h (d=80 °C) has the highest BET surface area (460 m^2/g) of all the pyrolyzed samples, shown from Table 4.3. 20 wt% Pyrolyzed 500°C 1h also has the largest pore volume (0.96 cm^2/g) of all the pyrolyzed samples. The BET surface area for 20 wt% Pyrolyzed 500°C 1h reproduced (157 m^2/g) is very much smaller than for 20 wt% Pyrolyzed 500°C 1h. The pore volume for 20 wt% Pyrolyzed 500°C 1h reproduced is approximately 1/3 of the pore volume for 20 wt% Pyrolyzed 500°C 1h. BET surface area for 20 wt% Pyrolyzed 600°C 1h is 316 m^2/g. Therefore, 20 wt% Pyrolyzed 600°C 1h has a lower BET surface area than 20 wt% Pyrolyzed 500°C 1h. 20 wt% Pyrolyzed 500°C 8h and 20 wt% Pyrolyzed 500°C 8h are both pyrolyzed over 8 hours and this results in the BET surface area 298 and 393 m^2/g, respectively. They have approximately equal pore volume and small difference in the pore size. The pore volume for 600°C 1h, 500°C 8h and 700°C 8h are approximately equal.

Catalyst 20 wt% pyrolyzed 400°C 1h has much smaller BET surface area than the other pyrolyzed samples. The pore volume for 400°C 1h also is much smaller than the pore volume for other pyrolyzed samples. The pore size for 400°C 1h is higher than the other pyrolyzed samples. It is approximately no difference in BET surface area, pore volume and pore sizes for 20 wt% pyrolyzed 400°C 1h at the degas temperature 80°C and 200°C, it is shown from Table 4.3. The pore volume and pore size for 20 wt% 400°C 1h are approximately equal for both the degas temperatures.

The surface area for 20 wt% pyrolyzed 500°C 1h reproduced increase from 157 m^2/g to 199 m^2/g when the degas temperature change from 80°C to 200°C. The Pore volumes are approximately equal for both the degas temperatures. The Pore size for 20 wt% pyrolyzed 500°C 1h reproduced is larger for degas temperature 200°C than for 80°C.

20 wt% pyrolyzed 400°C 1h (d=80°C) has the largest pores (18-19 nm). The other pyrolyzed catalyst (d=80°C) have pore sizes in the range 12.2-13.8 nm, this shows small change in pore volume.

The reason for the low degas temperature (80°C) was because analyzing of BET surface area and pore size distribution for the ambient dried samples. It was tried to use 100°C and 120°C, but these temperature decomposed the samples. The temperature 80°C was used because this temperature was equal to the temperature for drying in the furnace. The reason for the degas temperature 200°C was tested for 20 wt% pyrolyzed 400°C 1h and 20 wt% pyrolyzed 500°C 1h reproduced because see the difference in BET surface area, pore volume and pore size.

Only 10 % of the ambient dried sample was measured two times. BET and BJH method is a inexact technique because the technique is based on a lot of assumptions. More measurements for the each of the samples analyzed with BET and BJH method would give a better comparison for the BET surface area, pore volume and the pore sizes.

The surface of the ambient dried samples are the dried biopolymer. During the pyrolyze pores will be formed from the spaces from gases and liquids in the pyrolyze. This will make the surface for the pyrolyzed samples. (31)

4.2.2 TGA

TGA analyze was to determine the where and when reactions occurs. Mass loss% as function of temperature for the ambient dried samples in argon and it is shown in Figure 4.4. MS plot for 2.5wt% ambient dried in argon is shown in Figure 4.5. The other ambient dried samples follow the same MS-trends. In the MS-plot the intensity (logarithmic) is plotted as function of temperature (°C). The MS detector detected the following masses: 14, 15, 16, 17, 18, 28, 30, 32, 40, 44 and 46. These masses correlates to CH_2, CH_3, O^{2-}, OH^-, H_2O, CO, O_2, Ar, CO_2 and NO_2. The intensity of $CH3$ (red line), OH (purple line), H_2O (light blue line), CO (orange line), NO (green line) and CO_2 (dark blue line) were highest and therefore they are represent in the graphs. (Ar gives very high signals but is removed from the plot because it is the gas for the analyze).
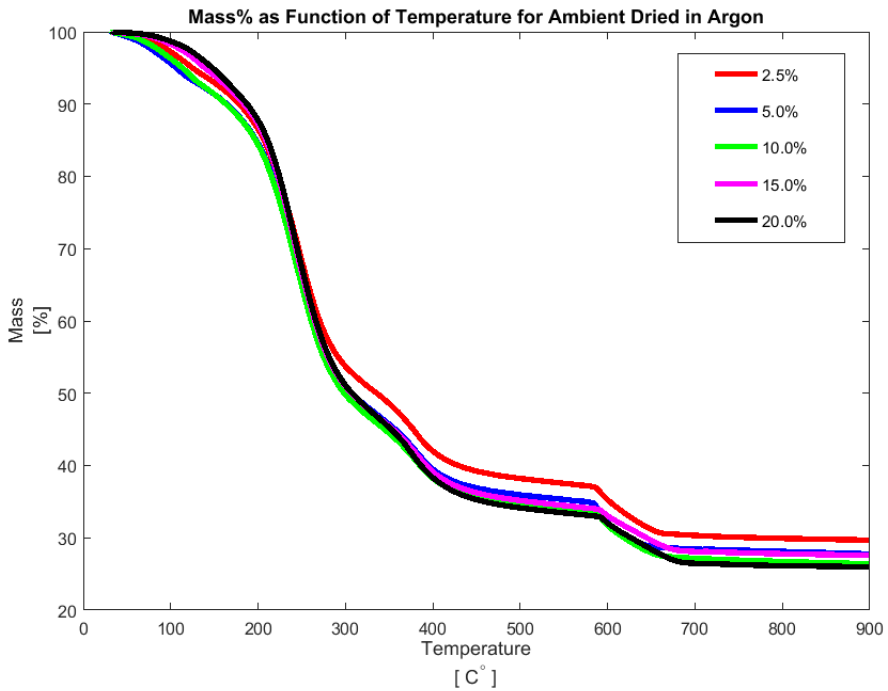
Figure 4.4: mass% as function of temperature (°C) for ambient dried samples in argon. Red line= 2.5 wt %, blue line=5.0 wt%, green line = 10 wt%, purple line = 15 wt% and black line= 20 wt%
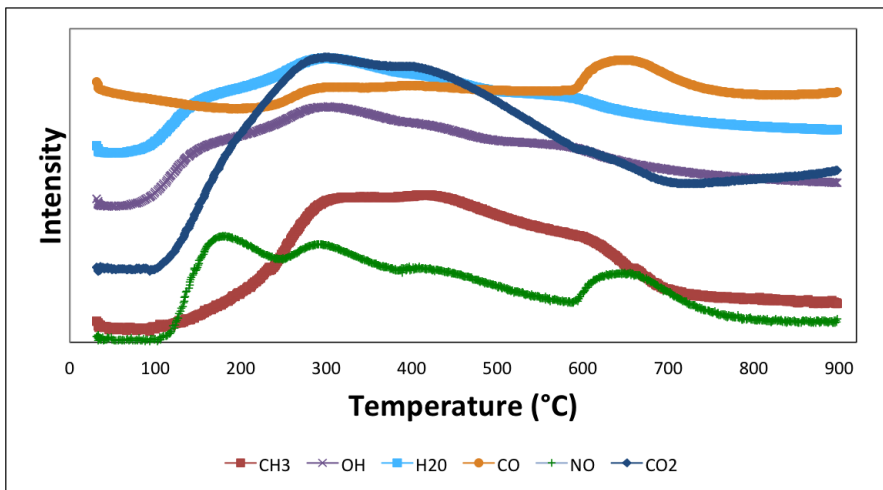
Figure 4.5: MS-data for 2.5 %wt ambient dried sample in argon.

The mass loss (%) decrease slowly from 30°C to 200°C, shown from Figure 4.4. This temperature range corresponds to high intensity of NO (green) and increase evolution of

gas CO_2 (dark blue), shown from Figure 4.5. From 200°C to 250°C there is a large drop in mass loss % from 85% to 50%, respectively. This large drop in mass loss corresponds to evolution of NO, CH_3, CO_2, H_2O and OH. From 250°C to 400°C the mass loss decrease slowly from 50% to 40%. From 400°C to 700°C there is small change in mass loss. The mass loss decrease slow linearly from 400°C to 600°C, in this range the increasing in evolution of NO, CH_3, OH and CO are relatively constant, but the evolution of CO_2 decrease. From 600°C to 700°C the evolution of CO and NO increase. Therefore the pyrolyze temperature range are 400-700°C.

The ambient dried samples follow the same trends, shown from Figure 4.4. The increase of alginate solution (wt%) follows to less mass loss during the temperature program. The rest mass at 900°C for all the ambient dried samples are approximately 30% of the original mass.

The samples were analyzed by TGA in air for estimating the loading of iron. Mass (%) as function of temperature for ambient dried samples in air is shown in Figure 4.6.
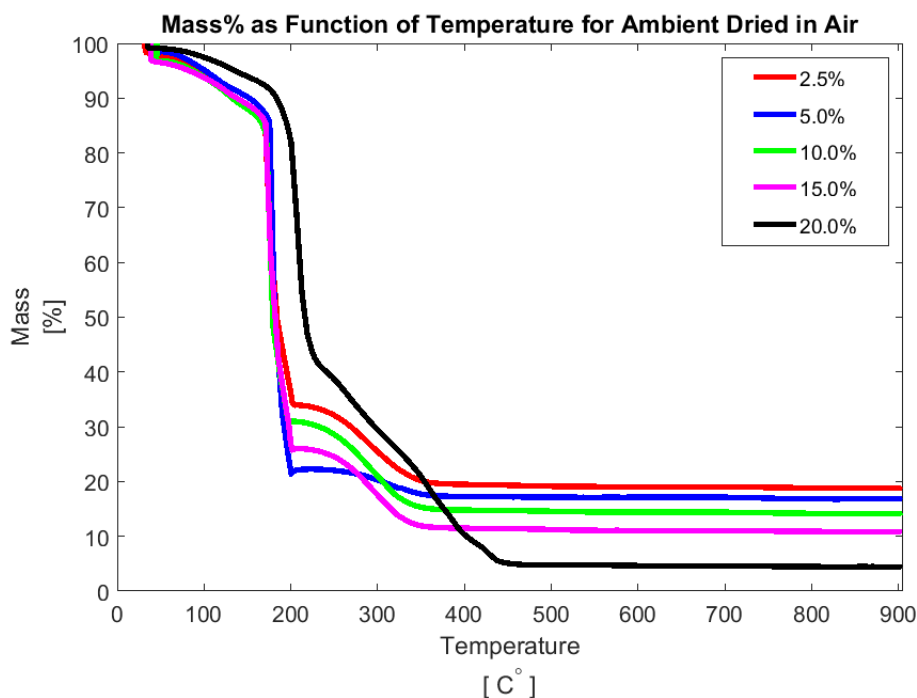
Figure 4.6: Mass% as function of Temperature (°C) for ambient dried samples in air. Red line= 2.5%, blue line=5.0%, green line = 10%, purple line = 15% and black line= 20%

The ambient dried samples in air follows the same trends, shown from Figure 4.6. All the ambient dried samples have very large mass loss in the temperature range 200-400°C. From the temperature 450-900°C the mass loss are constant. The amount of rest mass

follows the increase of alginate concentrations. The rest mass of 2.5, 5.0, 10, 15 and 20 wt% alginate are 18.7, 16.9, 14.2, 10.9 and 4.4 % of at 900°C are the original mass.

Mass (%) as function of temperature for pyrolyzed samples in air is shown in Figure 4.7. MS plot for pyrolyzed 400°C 1h in air is shown in Figure 4.8. The MS plot for the other pyrolyzed samples follows the same trends. The MS detector detected the following masses: 14, 15, 16, 17, 18, 28, 30, 32, 44 and 46. These masses correlates to CH_2, CH_3, O^{2-}, OH^-, H_2O, CO, O_2/NO, CO_2 and NO_2. The gases with highest intensity were OH (purple line) , H_2O (turquoise), CO_2 (dark blue line) and NO_2 (red line) and this is shown in Figure 4.8
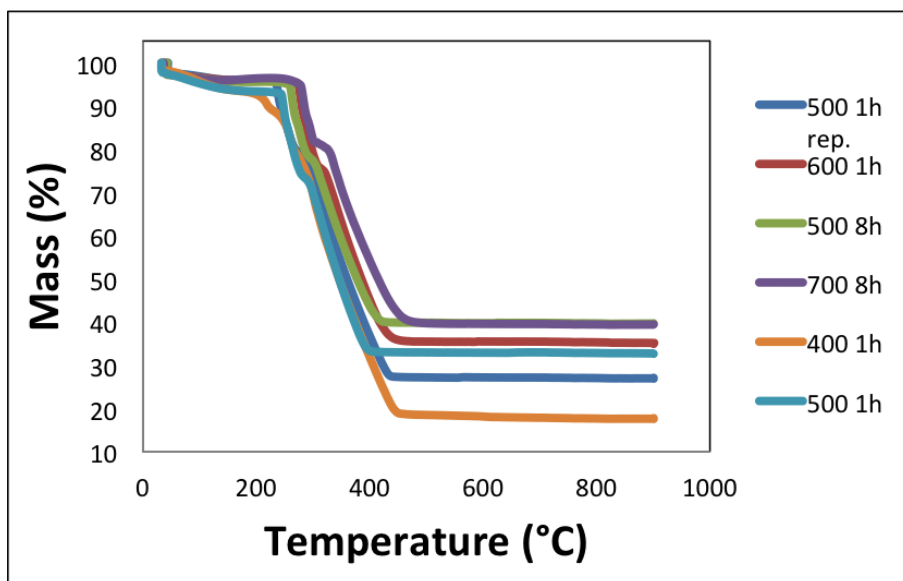
Figure 4.7: Mass (%) as function of Temperature (°C) for pyrolyzed samples in air.
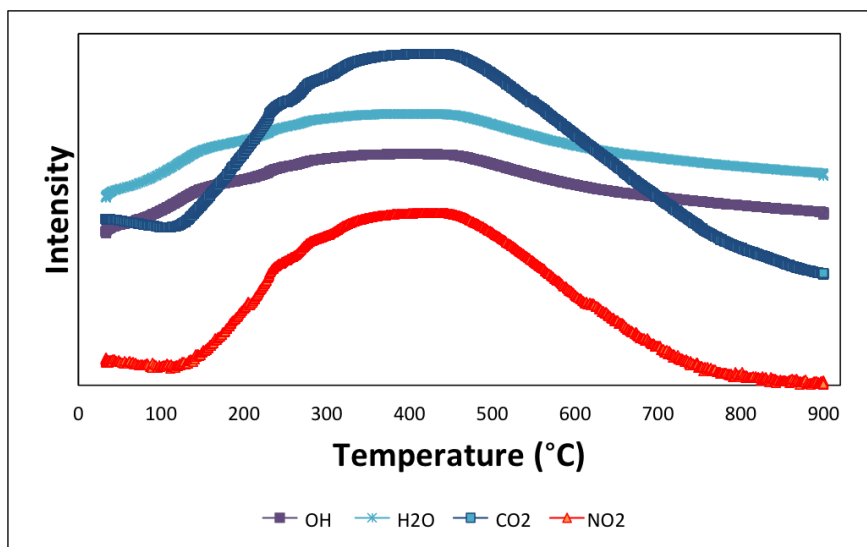
Figure 4.8: MS-data for20 wt% Pyrolyzed 400°C 1h in air.

All the pyrolyzed samples in air follows the same trends for mass loss as function of temperature, shown in Figure 4.7. The pyrolyzed samples have very large mass loss in the temperature range 200-400°C. The very large mass loss in 200-400°C corresponds to high evolution of NO_2 and CO_2.

The results from XRD gives the product Fe_2O_3 after pyrolyzing. The loading of iron for ambient dried and pyrolyzed samples are shown in Table 4.4. The estimating for loading of iron are based on the rest mass at 900°C and the calculations for the loading of iron is shown in Appendix C.

Table 4.4: Loading of iron for the ambient dried and pyrolyzed samples analyzed with TGA in air.

Sample	Loading of iron [wt%]
2.5 wt% Ambient dried	13.13
5.0 wt% Ambient dried	11.83
10 wt% Ambient dried	9.94
15 wt% Ambient dried	7.61
20 wt% Ambient dried	3.11
20 wt% Pyrolyzed 400°C 1h	12.26
20 wt% Pyrolyzed 500°C 1h	22.81
20 wt% Pyrolyzed 500°C 1h reproduced	18.78
20 wt% Pyrolyzed 600°C 1h	24.41
20 wt% Pyrolyzed 500°C 8h	27.65
20 wt% Pyrolyzed 700°C 8h	27.51

The loading of iron decrease with increase in alginate concentration. The pyrolyzed sam-

ples have larger loading of iron than the ambient dried samples because the hydrocarbons from the alginate are combusted during the pyrolyze. 20 wt% Pyrolyzed 400°C 1h and 20 wt% Pyrolyzed 500°C 1h have smaller iron loading than the other pyrolyzed samples.

4.2.3   ICP-MS

The results from ICP-MS gave highest concentration of iron, sodium and sulfur and this is shown in Table 4.5. Completed table for concentration for the elements: Fe, Na, Al, Si, P, S, Cl and Ca are shown in Appendix D.

Table 4.5: Concentration for iron, sodium and sulfur for the samples analyzed with ICP-MS.

Sample	Fe [wt%]	Na [wt%]	S [wt%]
Na alginate	0	9,28	0.18
2.5 wt% Ambient dried	12.90	0.02	0.06
5.0 wt% Ambient dried	11.29	0.02	0.08
10 wt% Ambient dried	10.64	0.02	0.08
15 wt% Ambient dried	10.19	0.06	0.05
20 wt% Ambient dried	6.0	0.21	0.05
20 wt% Pyrolyzed 400°C 1h	10.0	1.24	0.08
20 wt% Pyrolyzed 500°C 1h	27.40	0.25	0.18
20 wt% Pyrolyzed 500°C 1h reproduced	16.40	0.75	0.22
20 wt% Pyrolyzed 600°C 1h	28.36	0.38	0.27
20 wt% Pyrolyzed 500°C 8h	26.19	0.36	0.26
20 wt% Pyrolyzed 700°C 8h	26.55	0.57	0.23

The loading of iron is much larger for the pyrolyzed samples than for the ambient dried samples. The pyrolyzed samples have higher concentration of sodium than the ambient dried samples because some amount of the carbon is combusted. Sodium and sulfur are promotors for alginate.

4.2.4   Comparison of Iron Loading Results from TGA, ICP-MS and Theoretical Calculations

Comparison of iron loading results from TGA, ICP-MS and theoretical calculation for the different concentrations of iron alignate are shown in Figure 4.9.:
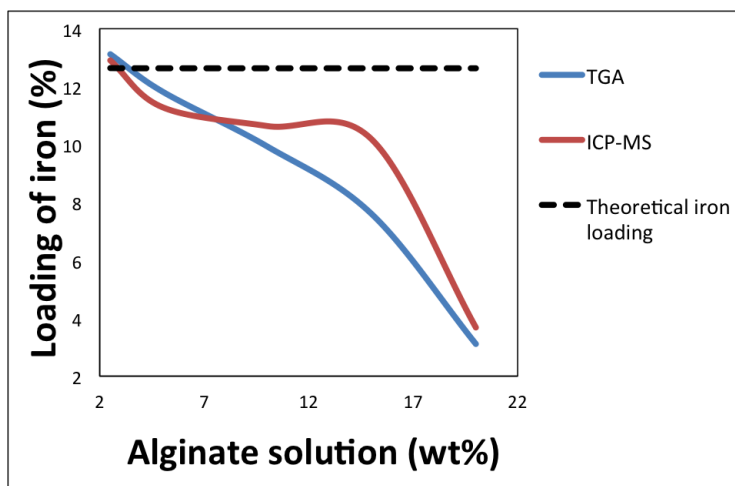
Figure 4.9: Loading of iron as function of Concentration of alginate solution (wt%) for TGA, ICP-MS and theoretical loading.

Theoretical loading of iron are 12.6 % for all the different concentrations of alginate. This is because the ratio for iron and alginate $(n_{Fe}/n_{alginate})$ are over 0.5 for all the different concentrations of alginate. The stochiometric ratio for iron and alginate are 1:2. Calculations for the theoretical loading of iron are shown in Appendix E.

Iron loading for TGA and ICP-MS follow approximately the same trends. TGA and ICP-MS have maximum loading of iron for 2.5 wt% for 13.13 and 12.90, this is a small amount higher than the theoretical calculation of iron loading. Iron loading based on TGA decrease gradually by increasing concentration of alginate. Iron loading based on ICP-MS decrease slowly from 2.5 to 15 wt% of alginate solution. Thereafter, the iron loading based on ICP-MS decrease very from 15 to 20 wt%.

4.2.5 XRD
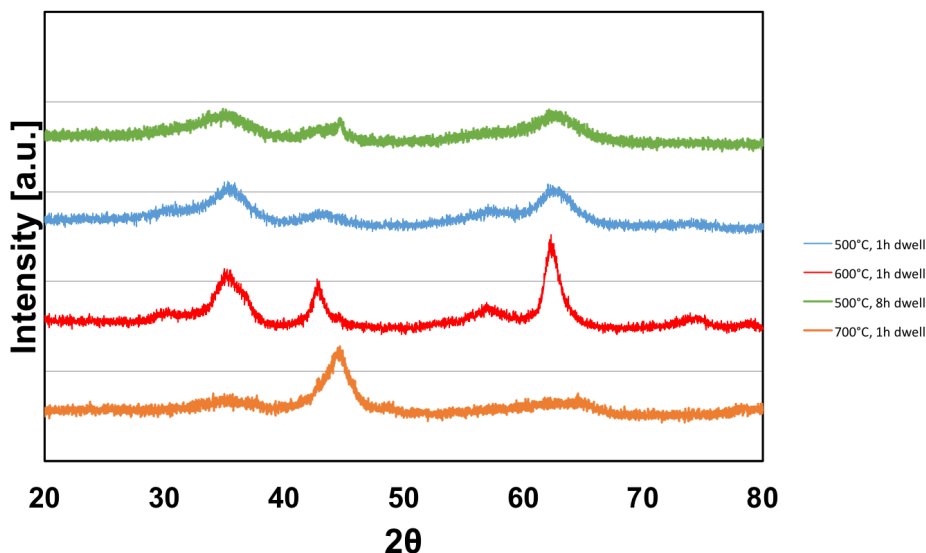
Figure 4.10: green line= 500°C dwelling 8 hours, blue line= 500°C dwelling 1 hour, red line= 600°C dwelling 1 hour, orange line= 700°C dwelling 8 hour.

XRD results shows the materials are amorphous, this is shown in Figure 4.10. The different pyrolyzed samples shows peaks in different angles of the spectrum. Carbon materials are amorphous is true described in Chapter 2.6.4.

4.2.6 S(T)EM

S(T)EM-EDX- elemental mapping was used to determine the fraction of the elements in the catalysts. The samples analyzed with S(T)EM were:

- 20 wt% Pyrolyzed 400°C 1h

- 20 wt% Pyrolyzed 500°C 1h

- 20 wt% Pyrolyzed 500°C 1h reproduced

For all the catalysts analyzed with S(T)EM-EDX elemental mapping it was selected to see the areas of iron and carbon in the samples. The S(T)EM-EDX-elemental mapping gives XRD spectrums for the elements in the catalyst. The S(T)EM-EDX-elemental mapping also gave fractions of the elements represents in the catalysts.

20 wt% Pyrolyzed 400°C 1h

20 wt% Pyrolyzed 400°C 1h was analyzed for the elements iron, carbon, sodium and oxygen.
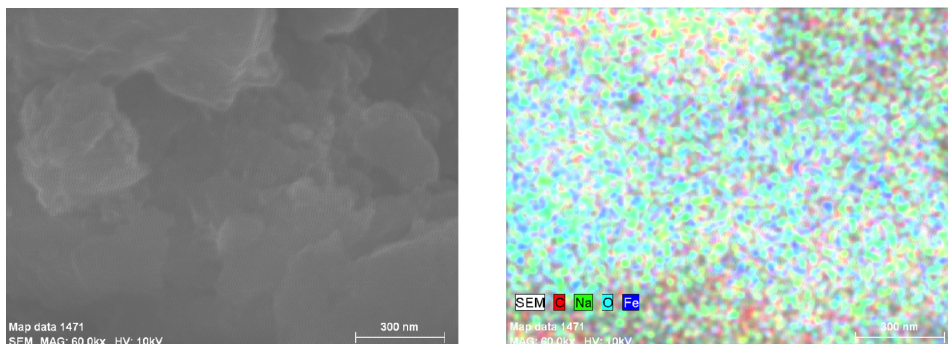
(a) SEM picture of 20 wt% Pyrolyzed 400°C 1h.

(b) SEM picture with areas for Fe, C, Na and O.

Figure 4.11: SEM pictures of 20 wt% Pyrolyzed 400°C 1h and element mapping.

SEM picture of 20 wt% Pyrolyzed 400°C 1h at 300 nm is shown in Figure 4.11a. Areas of iron (blue), carbon (red), sodium (green) and oxygen (turquoise) for 20 wt% Pyrolyzed 400°C 1h are shown in Figure 4.11b. Most of the SEM picture is areas of oxygen. Iron is finely distributed. The carbon areas in the sample are in the top and the bottom of the SEM picture shown from Figure 4.11b.

(a) Areas of iron

(b) Areas of carbon

(c) Areas of Oxygen

(d) Areas of Sodium
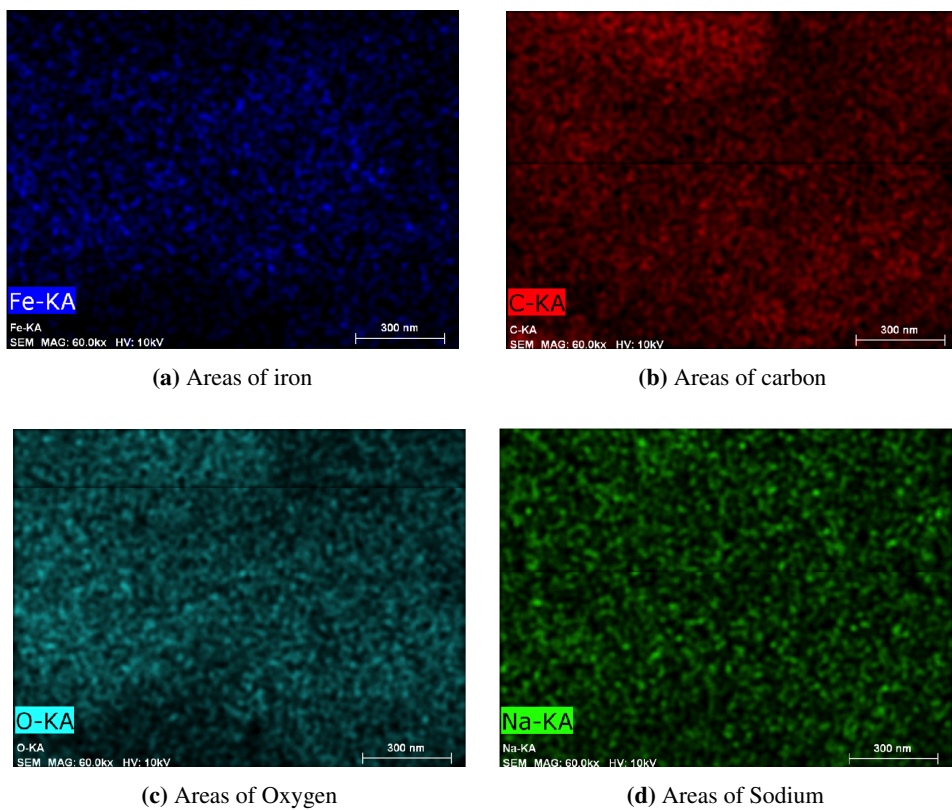
Figure 4.12: S(T)EM-EDX elemental mapping for 20 wt% Pyrolyzed 400°C 1h.
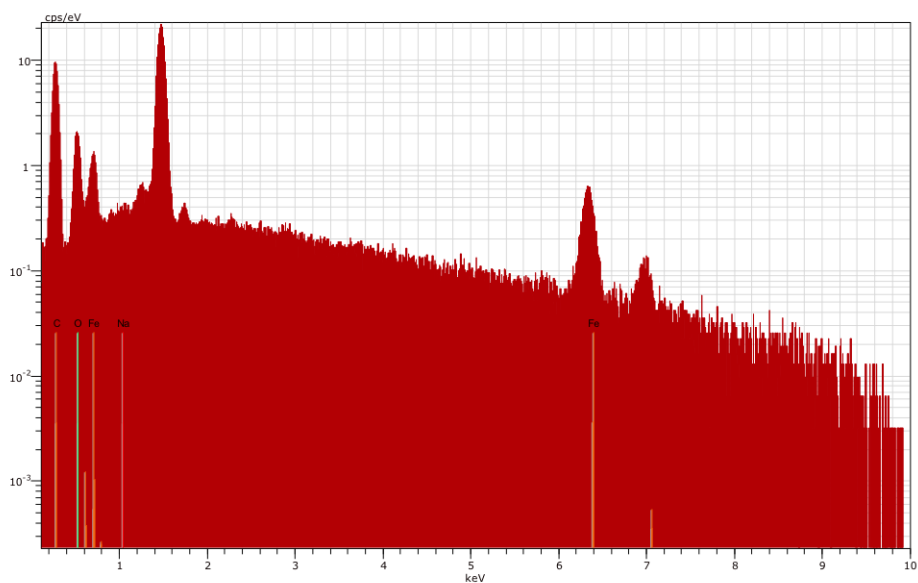
Figure 4.13: EDX spectrum for 20 wt% Pyrolyzed 400°C 1h.

Table 4.6: Fraction of elements represents in 20 wt% Pyrolyzed 400°C 1h.

Sample	Elements represents in the samples [wt%]
Fe	24.5
C	30.2
O	43.1
Na	2.2

20 wt% Pyrolyzed 500°C 1h

20 wt% Pyrolyzed 400°C 1h was analyzed for the elements iron, carbon, aluminum and oxygen.
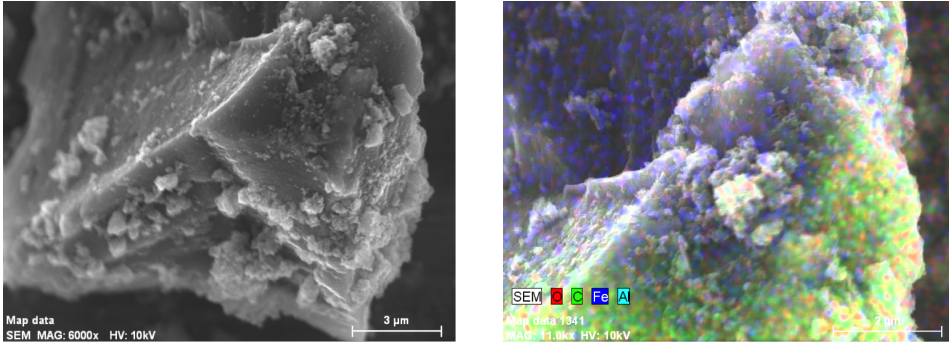
(a) SEM picture of 20 wt% Pyrolyzed 500°C 1h.

(b) SEM picture with areas for Fe, C, O and Al.

Figure 4.14: SEM pictures of 20 wt% Pyrolyzed 500°C 1h and element mapping

SEM picture of 20 wt% Pyrolyzed 500°C 1h at 3 μm is shown in Figure 4.14a. Areas of iron (blue), carbon (green), oxygen (red) and aluminum (turquoise) for 20 wt% Pyrolyzed 400°C 1h are shown in Figure 4.14b. Most of the SEM picture is areas of carbon. Iron is finely distributed. The carbon areas in the sample are in the bottom of the SEM picture shown from Figure 4.11b. The areas of aluminum is from the plate for S(T)EM.

(a) Areas of iron

(b) Areas of carbon

(c) Areas of oxygen

(d) Areas of aluminum
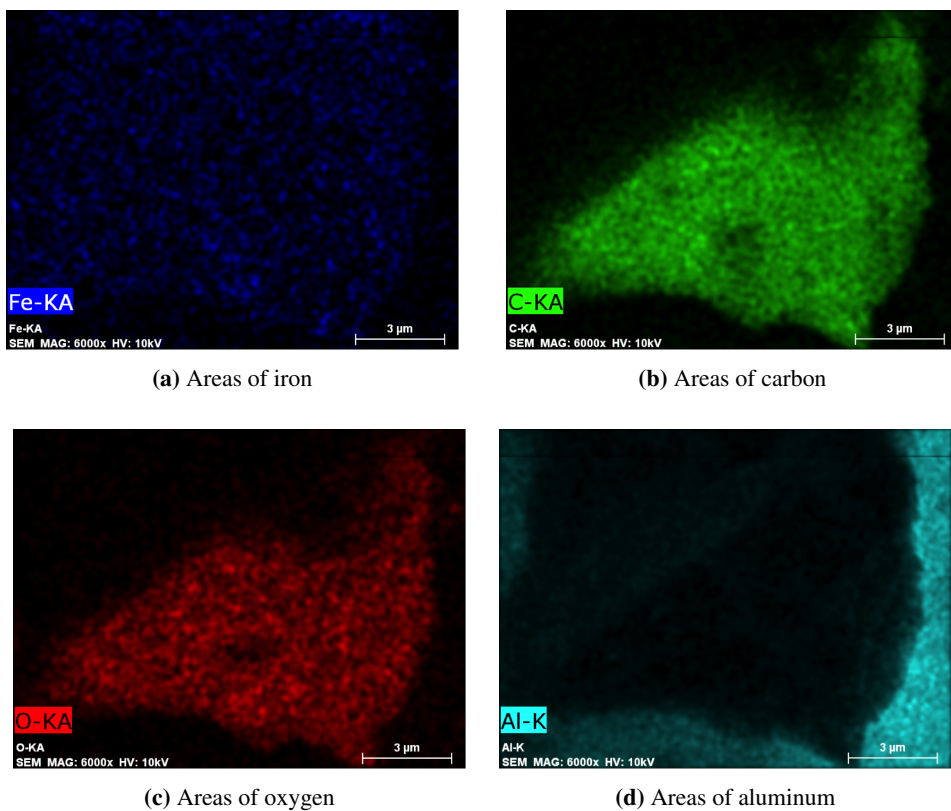
Figure 4.16: S(T)EM-EDX elemental mapping for 20 wt% Pyrolyzed 500°C 1h.
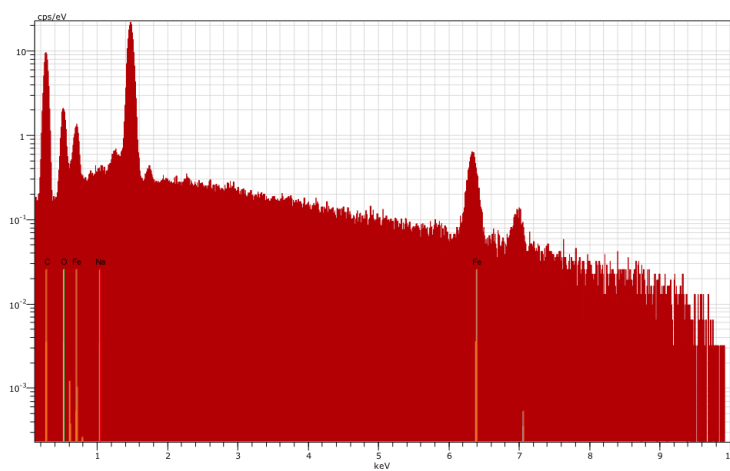
Figure 4.17: EDX spectrum for 20 wt% Pyrolyzed 500°C 1h.

Table 4.7: Fraction of elements represents in 20 wt% Pyrolyzed 500°C 1h.

Sample	Elements represents in the samples [wt%]
Fe	28.0
C	54.7
Al	17.0
O	0.3

20 wt% Pyrolyzed 500°C 1h reproduced

20 wt% Pyrolyzed 500°C 1h reproduced was analyzed for the elements iron, carbon, sodium and oxygen.
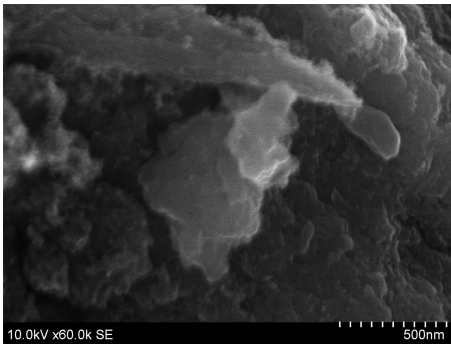
(a) SEM picture of 20 wt%
Pyrolyzed 500°C 1h reproduced
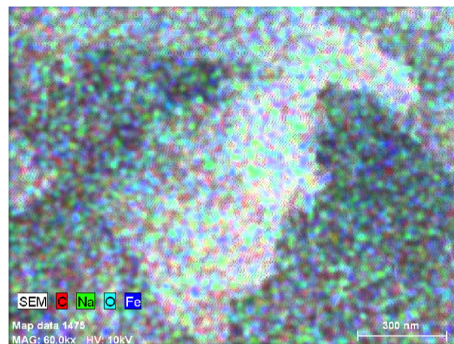
(b) SEM picture with areas for
Fe, C, Na and O.

Figure 4.18: SEM pictures of 20 wt% Pyrolyzed 500°C 1h reproduced and element mapping.

SEM picture of 20 wt% Pyrolyzed 500°C 1h reproduced at 500 nm is shown in Figure 4.18a. Areas of iron (blue), sodium (green), carbon (red) and oxygen (turquoise) for 20 wt% Pyrolyzed 500°C 1h reproduced are shown in Figure 4.18b. Iron is finely distributed and the concentration of oxygen is high, shown from Figure 4.18b. 20 wt% Pyrolyzed 500°C 1h reproduced has small concentration of carbon.

(a) Areas of iron

(b) Areas of carbon

(c) Areas of oxygen

(d) Areas of sodium
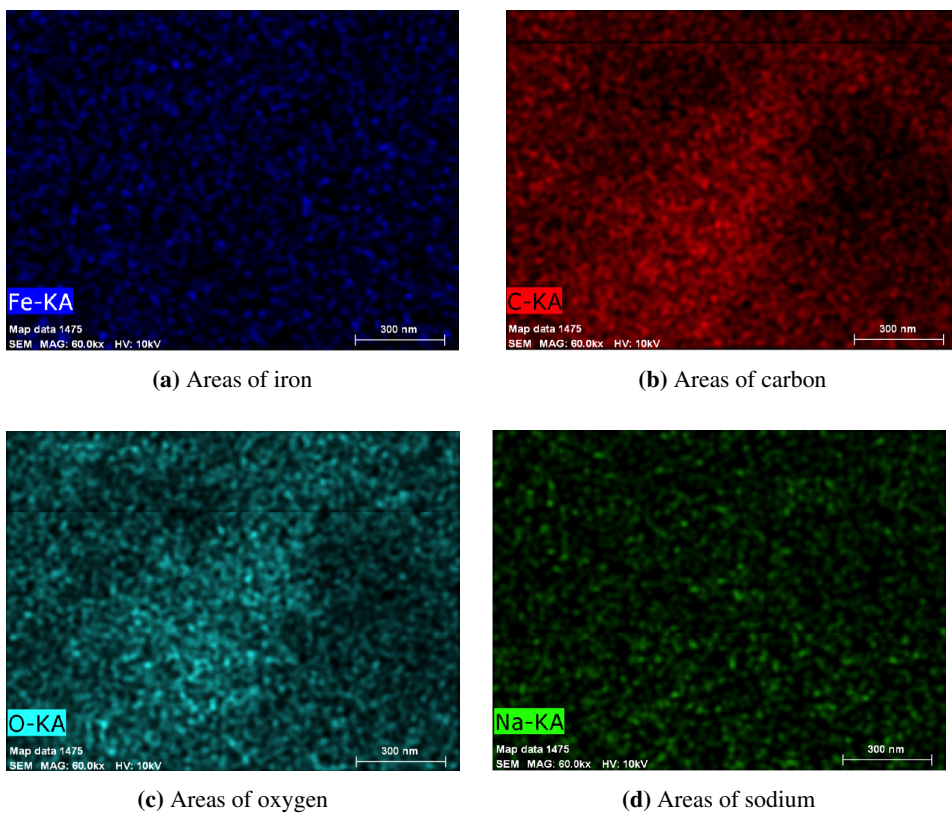
Figure 4.19: S(T)EM-EDX elemental mapping for 20 wt% Pyrolyzed 500°C 1h reproduced.
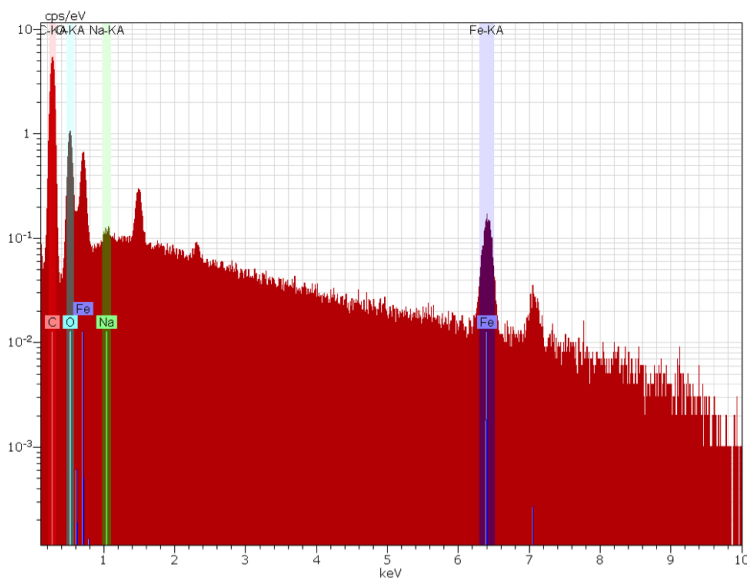
Figure 4.20: EDX spectrum for 20 wt% Pyrolyzed 500°C 1h reproduced.

Table 4.8: Fraction of elements represents in 20 wt% Pyrolyzed 500°C 1h reproduced.

Sample	Elements represents in the samples [wt%]
Fe	26.
C	0
O	71.5
Na	2.6

4.3   Catalyst Testing

The catalysts were tested at low and high pressure. From now the 20 wt% pyrolyzed in the different temperatures and dwell time. The names of the catalysts will now be referred to:

- 20 wt% Pyrolyzed 400°C 1h = 400°C 1h

- 20 wt% Pyrolyzed 500°C 1h = 500°C 1h

- 20 wt% Pyrolyzed 500°C 1h reproduced = 500°C 1h rep.

- 20 wt% Pyrolyzed 500°C 8h = 500°C 8h

- 20 wt% Pyrolyzed 600°C 1h = 600°C 1h

- 20 wt% Pyrolyzed 700°C 8h = 700°C 8h

- Reference Catalyst

4.3.1 Low Pressure Fischer-Tropsch (LPFT) Test

The conditions for the low pressure FT test, were 340°C and 1 bar. For the low pressure test the following pyrolyzed samples were tested:

- 500°C 8h

- 700°C 8h

The activity and the selectivity of the catalysts were tested at the flow ratios H_2:CO 1:1 and 10:1. When the flow ratio was 1:1 the composite for the flow was H_2:CO:Ar 1.5:1.5:47 mL/min. When the flow was 10:1 the composite for the flow was H_2:CO:Ar 15:1.5:33.5 mL/min. The conversions at the different ratios of the flows are shown in Table 4.9:

Table 4.9: CO conversion for the different catalysts tested with low pressure FT.

Sample	CO conversion at H_2:CO 1:1 [%]	CO conversion at H_2:CO 10:1 [%]
500°C 8h	5.0	10.0
700°C 8h	-	8.0

The CO conversions value (10.0 and 8.0 %) for 500°C 8h and 700°C 8h are in the same order of magnitude.

The products produced in the low pressure test are CH_4, $C_2 - C_4$- total olefins, $C_2 - C_4$ total parafins and C5+ hydrocarbons. CO_2 is not included in the product distribution because insufficient calibration of CO_2 for the LPFT system. Carbon selectivity (%) within hydrocarbon products as function of product distribution for 500°C 8h at both the flow ratios 1:1 and 10:1 are shown in Figures 4.21a and 4.21b, respectively.
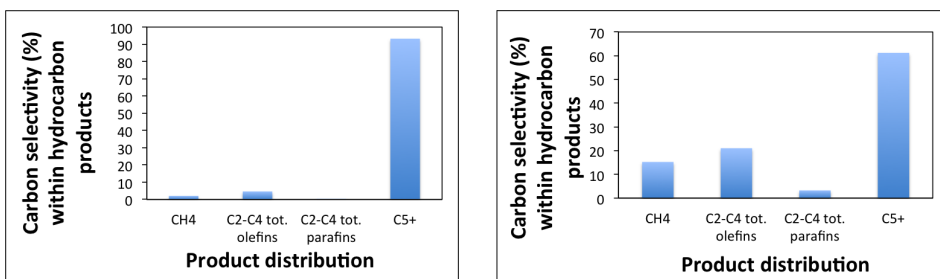
(a) Carbon selectivity (%) as function of product distribution for 500°C 8h 1:1 (340°C 1 bar)

(b) Carbon selectivity (%) as function of product distribution for 500°C 8h 10:1 (340°C 1 bar)

Figure 4.21: Carbon selectivity (%) within hydrocarbon products for 500°C 8h flow ratio (1:1) and (10:1) (340°C 1 bar).

Catalyst 500°C 8h at the flow ratio 1:1 produce mainly C5+ (93.3 %) hydrocarbons, this is shown from Figure 4.21a. 500°C 8h at the flow ratio 1:1 produce small amounts of CH_4 (2.0 %) $C_2 - C_4$- total olefins (4.6 %) and $C_2 - C_4$ total parafins (0.1 %), shown from Figure 4.21a. Catalyst 500°C 8h with the flow ratio 10:1 produce most C5+ (61.2 %), shown from Figure 4.21b. The product distribution for $C_2 - C_4$ total olefins is 21.0% and $C_2 - C_4$ total parafins 3.2%. The carbon selectivity for CH_4 is 15.2%, shown from Figure 4.21b.

Carbon selectivity (%) as function of product distribution for 700°C 8h at the flow 10:1 is shown in Figure 4.22:
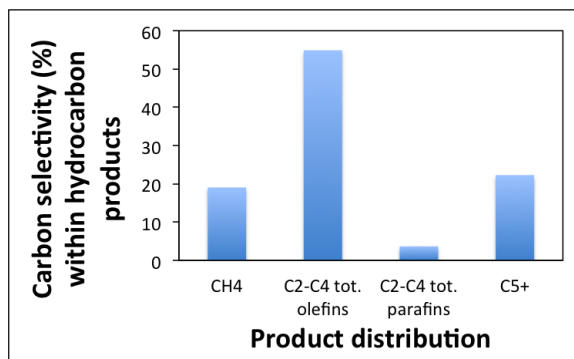
Figure 4.22: Carbon selectivity (%) within hydrocarbon products as function of product distribution for 700°C 8h at the flow ratio 10:1 (340°C 1 bar)

Catalyst 700°C 8h at the flow ratio 10:1 produce most $C_2 - C_4$ total olefins (54.9 %), this is shown from Figure 4.22. The production of $C_2 - C_4$ total parafins and C5+ are 3.7 % and 22.3 %, respectively. The carbon selectivity for CH_4 is 19%.

Catalyst 500°C 8h produce most C5+ for both the flow ratios (1:1 and 10:1). 500°C 8h produce only mainly C5+ at the flow ratio 1:1. The distribution of CH_4, $C_2 - C_4$ total olefins and $C_2 - C_4$ total parafins for 500°C 8h are larger at the flow ratio 10:1 than 1:1. 700°C 8h (10:1) produce most $C_2 - C_4$ total olefins. 700°C 8h has smaller distribution of C5+ than 500°C 8h (1:1 and 10:1). 700°C 8h has higher distribution of CH_4 than 500°C 8h (1:1 and 10:1).

4.3.2 High Pressure Fischer-Tropsch (HPFT) Test

The conditions for the high pressure FT test, were 340°C and 20 bar. For the High pressure FT the following pyrolyzed samples were tested:

- 400°C 1h

- 500°C 1h

- 500°C 1h reproduced

- 600°C 1h

- 700°C 8h

- Reference Catalyst

CO conversion (%) as function of Time (h) for the different pyrolyzed catalysts tested with high pressure are shown in Figure 4.23.
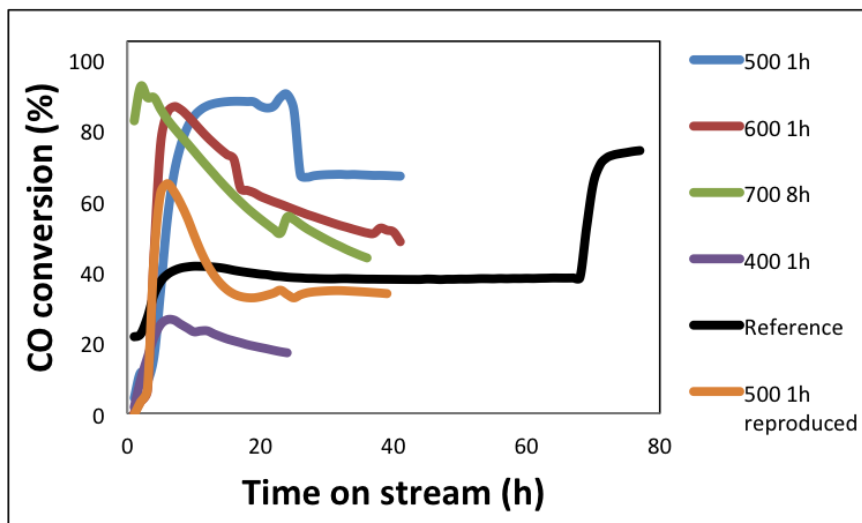
Figure 4.23: CO conversion (%) as function of Time (h) for the different catalysts tested with high pressure FT (340°C 20 bar).

Only 500°C 1h and 500°C 1h reproduced of the produced catalyst are at steady state. The samples are at steady state when there is no change in the conversion. 500°C 1h is at steady state at 19 (88 %) and 41 hours (67 %). 500°C 1h is a very active catalyst because high the conversion (88 %) and at steady state at the same time. The flow was increased from 269.4 mL/min to 299.3 mL/min after 20 hours because the catalyst was at steady state. The change in flow first resulted in decrease the conversion. Thereafter, the conversion increased to 90 %. At 25 hours the flow was changed to 598.6 mL/min this followed the conversion decreased very fast from 86 % to 67 % in one hour. The conversion for 500°C 1h obtain steady state at 67 %. The changing of flow for 500°C 1h are shown in Figure 4.24.

The catalyst 700°C 8h has very high conversion (92 %) after 2 hours and then the conversion decrease fast to 50 % conversion at 22 hours. The CO conversion for 700°C 8h increased after 22 hours up to 55 % conversion because the temperature was adjusted from 343°C to 340°C. Further the conversion decreased slowly to 44% at 35 hours. The testing of 700°C 1h was stopped after 35 hours because deactivation. The flow for 700°C 8h during the reaction was 250 mL/min.

The catalyst 600°C 1h increase fast to the conversion 86 % after 6 hours and then then decrease linearly to 72 % conversion after 16 hours. At 16 hours the temperature was adjusted from 343°C to 340°C because exothermic reactions. The decreasing in temperature shows a significant drop in conversion from 72% to 64% between 16 to 17 hours. Thereafter, the conversion of 600°C 1h decrease slowly linearly from 64 to 50% at 35 hours. After 35 hours the temperature was increased from 338°C to 340°C so the conversion increased from 50 to 52% After 42 hours the testing of 600°C 1h was stopped because deactivation of the catalysts. The flow for 600°C 1h during the reaction was 250 mL/min.

The catalyst 500°C 1h reproduced has significant lower conversion than 500°C 1h. 500°C 1h reproduced increase fast to the highest conversion 65 % after ca. 5 hours and then decrease to steady state conversion of 34% after 15 hours. 500°C 1h reproduced has a small "jump" at 25 hours. This is because the temperature was adjusted from 342°C to 340°C because exothermic reactions. The testing of 500°C 1h was stopped after 40 hours because the syngas bottle was empty. The flow for 500°C 1h during the reaction was 250 mL/min.

The catalyst 400°C 1h obtained the highest conversion 26% after 10 hours and then decrease linear slowly to 17% after 23 hours. The testing of 400°C 1h was stopped after 23 hours because very low conversion. The flow for 400°C 1h during the reaction was 250 mL/min.

The reference catalyst obtained steady state at 14 hours with the conversion 41 %. The conversion of the reference catalyst varied from 41 to 37% from 14 to 70 hours. The flow was changed from 250 mL/min to 125 mL/min after 70 hours. The changing in flow followed to the conversion increased from 38 to 71% in 2 hours. The reference catalyst obtained steady state at 71 % at 93 hours. The testing of the reference catalyst was stopped after 93 hours. CO conversion (%) as function of Time (h) for 500°C 1h is shown in Figure 4.24.
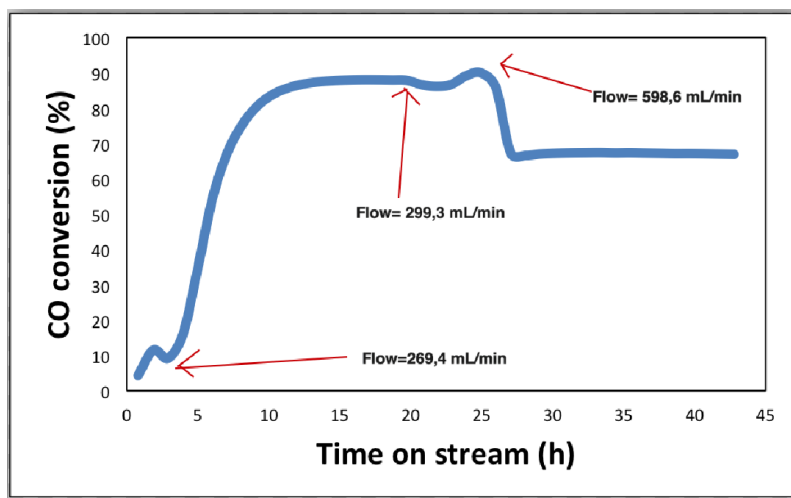
Figure 4.24: CO conversion (%) as function of time (h) for 500°C 1h (340°C 20 bar).

Catalyst 500°C 1h is at steady state at 19 and 41 hours and this gave the Gas Hourly Space Velocity (GHSV) values 32 328 and 71 832, respectively. GHSV are calculated from Matlab program during the High Pressure FT testing and the GHSV are also calculated manually. The manually calculations are shown in Appendix F.

Carbon selectivity (%) within hydrocarbon products as function of GHSV for the steady state ranges for 500°C 1h are shown in Figure 4.25. FT selectivity shows the products CH_4, $C_2 - C_4$ total parafins, $C_2 - C_4$ olefins and C5+. CO_2 is also a product in high pressure FT, but CO_2 is taken away from the FT selectivity.
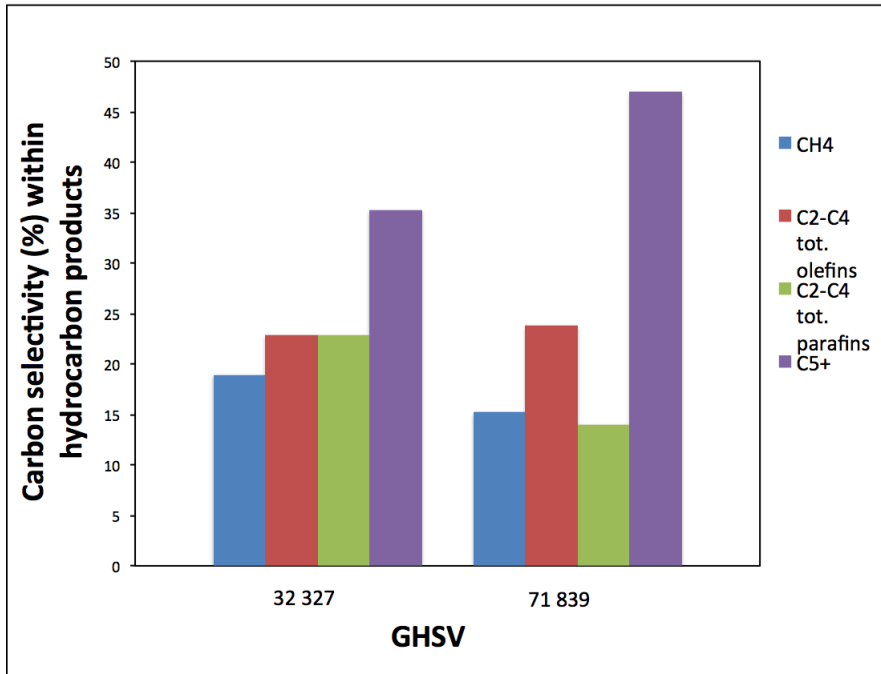
Figure 4.25: Carbon selectivity (%) within hydrocarbon products as function of GHSV for 500°C 1h at the GHSV 32 328 and 71 832 (340°C 20 bar).

At GHSV 32 327 for 500°C 1h the distribution of $C_2 - C_4$ total olefins are equal to $C_2 - C_4$ total parafins, both corresponds to 23 % of the carbon selectivity. At GHSV 32 327 the distribution of CH_4 is 19 % of the carbon selectivity and C5+ compose to 35% of the carbon selectivity. The 500°C 1h produce most C5+ hydrocarbons at GHSV 71 839. This corresponds to 47% of the carbon selectivity. The carbon selectivity for $C_2 - C_4$ total olefins and $C_2 - C_4$ total parafins are 24% and 14 % of the distribution. The carbon selectivity for CH_4 at 71 839 at is 15 %.

500°C 1h produce most C5+ at both 32 327 and 71 839. The distribution of $C_2 - C_4$ total olefins are approximately equal for both steady state ranges. 500°C 1h produce less $C_2 - C_4$ total olefins at 71 839 than 32 327.

The reference catalyst was steady state at 14 and 93 hours and this shows to GHSV 60000 and 30000. The carbon selectivity (%) as function of GHSV for the steady state ranges for the reference catalyst are shown in Figure 4.26:
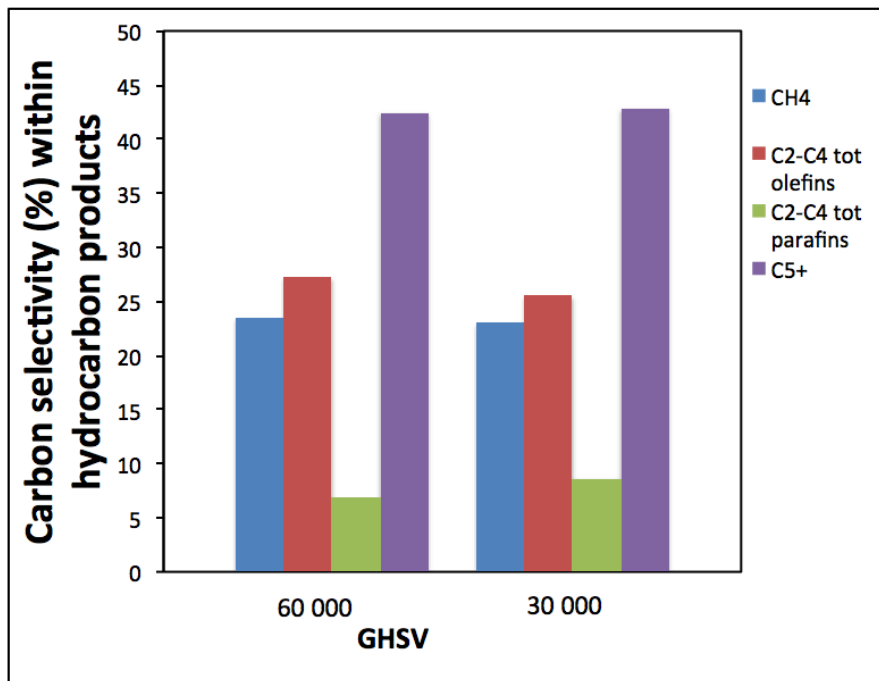
Figure 4.26: Carbon selectivity (%) within hydrocarbon products as function og GHSV for the reference catalysts at the GHSV 60 000 and 30 000 (340°C 20 bar).

The carbon selectivity for the reference catalyst at GHSV 60 000 are 23 % CH4, 27% $C_2 - C_4$ total olefins, 7 % $C_2 - C_4$ total parafins and 42% C5+. The carbon selectivity for the reference catalyst at GHSV 30 000 are 23% CH4, 25% $C_2 - C_4$ total olefins, 8 % $C_2 - C_4$ total parafins and 43% C5+. Therefore reference catalyst produce equal fraction of CH4 and C5+ at 60 000 and 30 000. The difference between the carbon selectivity for 60 000 and 30 000 are the fraction of produced $C_2 - C_4$ total olefins and $C_2 - C_4$ total parafins.

Catalyst 500°C 1h and the other pyrolyzed catalysts are compared at equal GHSV and conversion. Since the GHSV for CO conversion and Iron Time Yield FTY for all the catalysts are compared and shown in Table 4.10. FTYs are calculated from Equation F and the calculations are shown in Appendix F. FTYs are adjusted by the iron loading from ICP-MS.

Table 4.10: GHSV, CO conversion (%) and FTY for all samples tested at FT (340°C, 20 bar).

Sample	Iron loading [%]	GHSV [cm^3/g min]	CO conversion [%]	FTY * [$molCO/g_{Fe}s$]
20 wt% Pyrolyzed 400°C 1h	10.0	60 000	26	$5.1 \cdot 10^{-4}$
20 wt% Pyrolyzed 500°C 1h	27.4	71 839	67	$5.2 \cdot 10^{-4}$
20 wt% Pyrolyzed 500°C 1h reproduced	16.4	60 000	65	$7.2 \cdot 10^{-4}$
20 wt% Pyrolyzed 600°C 1h	28.4	60 000	64	$4.0 \cdot 10^{-4}$
20 wt% Pyrolyzed 700°C 8h	26.6	60 000	65	$4.4 \cdot 10^{-4}$
Reference Catalyst	92.0	60 000	42	$7.9 \cdot 10^{-5}$

FTY values at GHSV and CO conversion at 60 000 $cm^3/gmin$ and 65 %, respectively.

FTY for 500°C 1h, 400°C 1h, 600°C 1h and 700°C 8h are approximately equal. FTY for 500°C 1h reproduced is somewhat larger than 500°C 1h, 400°C 1h, 60°C 1h and 700°C 8h. The reference catalyst has lower FTY than the other tested catalyst, shown from Table 4.10. 500°C 1h reproduced deactivate at CO conversion 65 % so the high FTY means the iron particles are very active when they deactivate.

Carbon selectivity (%) within hydrocarbon products as function of GHSV for all the tested catalyst are shown in Figure 4.27:
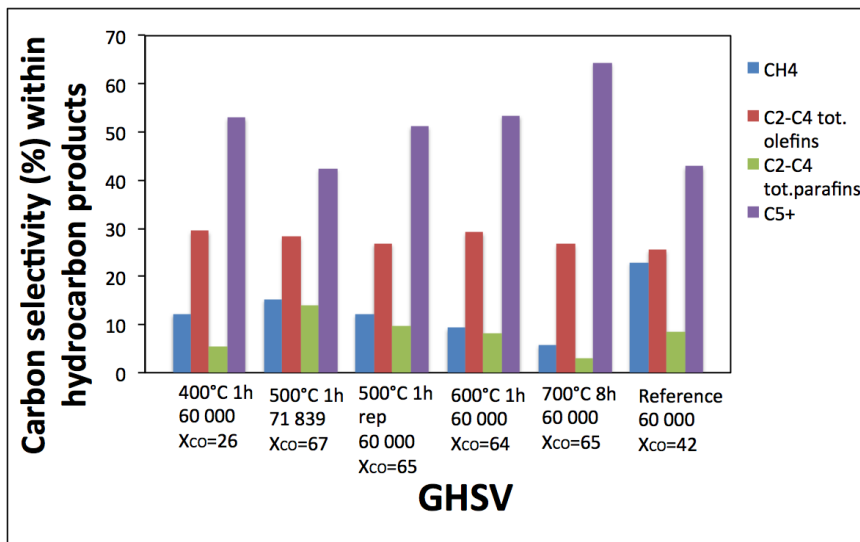
Figure 4.27: Carbon selectivity (%) within hydrocarbon products as function of GHSV for all the catalyst tested with high pressure FT (340°C 20 bar).

All the tested catalysts at HPFT have highest distribution of C5+, shown from Figure 4.27.

The distribution of $C_2 - C_4$ total olefins are approximately constant for all the tested catalyst (around 30 %). The distribution of CH_4 and $C_2 - C_4$ total parafins decrease by higher pyrolyze temperature for the produced catalyst. The reference catalyst has much higher distribution of CH_4 and $C_2 - C_4$ total olefins than the produced catalysts.

Carbon selectivity (%) as function of GHSV for all the tested catalyst are shown in Figure 4.28. In this Figure 4.28 the carbon selectivity (%) CO_2 is included with CH_4, $C_2 - C_4$ total olefins, $C_2 - C_4$ total parafins and C5+.
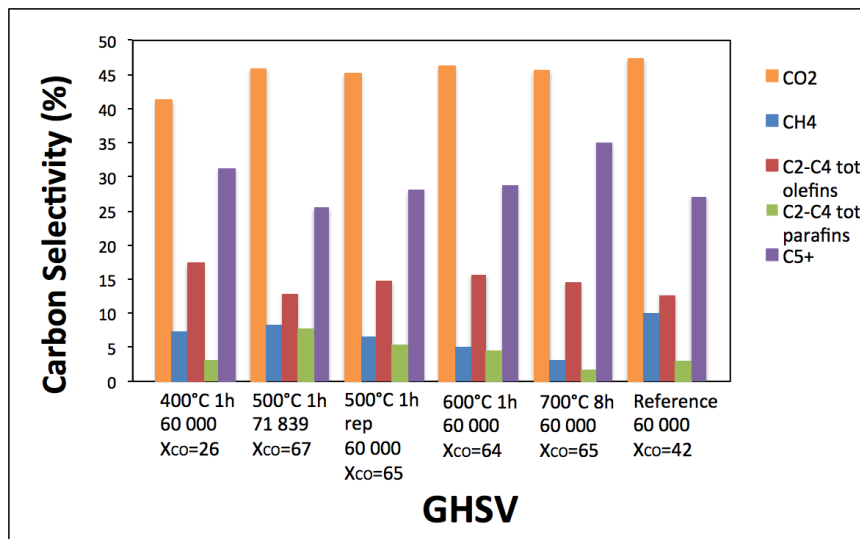
Figure 4.28: Carbon selectivity (%) as function of GHSV for all the catalyst tested with HPFT. (340°C, 20 bar).

All the tested catalyst have highest carbon selectivity of CO_2, shown from Figure 4.28. Thereafter, the carbon selectivity C5+ are second highest.

Carbon selectivity within hydrocarbon products as function of CO conversion (%) are plotted for d 500°C 1h and 600°C 1h and they are shown in Figures 4.29a and 4.29b, respectively. Carbon selectivity within hydrocarbon products as function of CO conversion (%) were plotted for understanding the different between carbon selectivity for a steady state and a deactivation catalysts. 600°C 1h follow the same trends as the other deactivation catalysts.
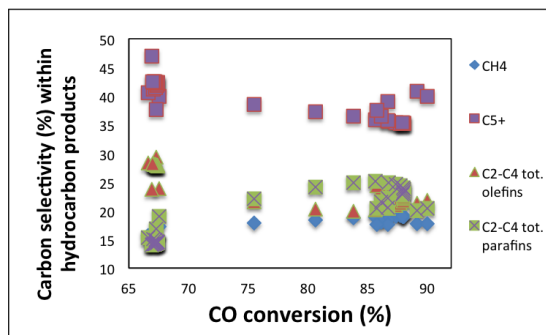
(a) Carbon selectivity (%) as function of CO conversion (%) for 500°C 1h.
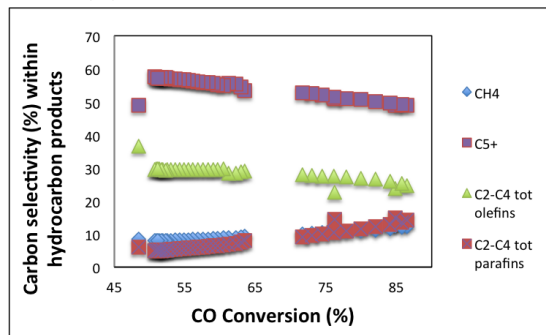
(b) Carbon selectivity (%) as function of CO conversion (%) for 600°C 1h

Figure 4.29: Carbon selectivity (%) within hydrocarbon products as function of CO conversion (%) for a steady state and a deactivation catalysts.

Catalyst 500°C 1h produce most C5+ at 66-67 % and the distribution of C5+ decrease for higher conversions. This is shown from Figure 4.29a. The distribution of CH_4, $C_2 - C_4$ total olefins and $C_2 - C_4$ total parafins are low and random for all conversions. The deactivation catalyst 600°C 1h has linearly less production of C5+ and C_2-C_4 total olefins for higher conversions, shown from Figure 4.29b . The production of CH_4 and $C_2 - C_4$ total parafins increase for higher conversions. The deactivation catalyst 600°C 1h has a more clearly distribution of the produced hydrocarbons. The hydrocarbon distribution are

more random for 500°C 1h.

4.3.3 Analyzing with TEM of HPFT-samples

The samples tested at FT were analyzed with TEM both before and after the testing. The samples were tested because analyzing of the particle distribution.

The samples analyzed with TEM before and after testing in the HPFT were:

- 500°C 1h

- 600°C 1h

- 700°C 8h

TEM pictures of 500°C 1h before and after testing at FT are shown in Figures 4.30a and 4.30b, respectively. The particles are mainly spherical before the testing. The particles growth during the reaction. After the testing the particles are spherical and oval. The particle size are larger after the reaction.
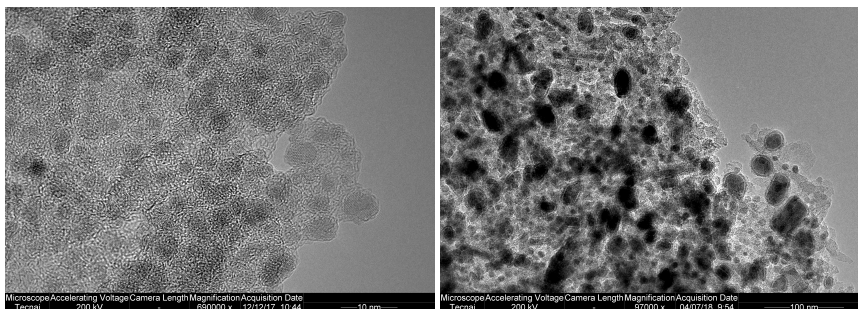
(a) TEM picture of 500°C 1h before tested in HPFT. TEM picture taken in China

(b) TEM picture of 500°C 1h after testing in HPFT. TEM picture taken in China

Figure 4.30: TEM pictures for 500°C 1h before and after testing in HPFT

The iron particles (black areas) are finely distributed, this is shown in Figure 4.30a. The iron particles grows together during the reaction are shown in Figure 4.30b. The black areas of iron particles are much larger after the reaction, shown in Figure 4.30b. 600°C 1h and 700°C 8h follow the same trends and the TEM picture for them are shown in Appendix G. The particle distribution for catalyst 500°C 1h are better distributed than 600°C 1h and 700°C 8h, this is shown in Figures 4.30a, G.1a and G.2a. The particle in catalyst 700°C 8h is sintered because the high temperature, this is shown from G.2a. (The Figures G.1a and G.2a are in Appendix G.)

The particle size distribution for the samples tested in high pressure FT and analyzed with TEM were measured with ImageJ. Frequency (%) as function of diameter of the particles

(nm) are shown in the Figures 4.31a - 4.33b. The particle size distribution for 500°C 1h are shown in Figures 4.31a and 4.31b. Figure 4.31a shows the particle size distribution before the reaction and Figure 4.31b shows after the reaction.

(a) 500°C 1h before testing in the HPFT.

(b) 500°C 1h after testing in the HPFT.
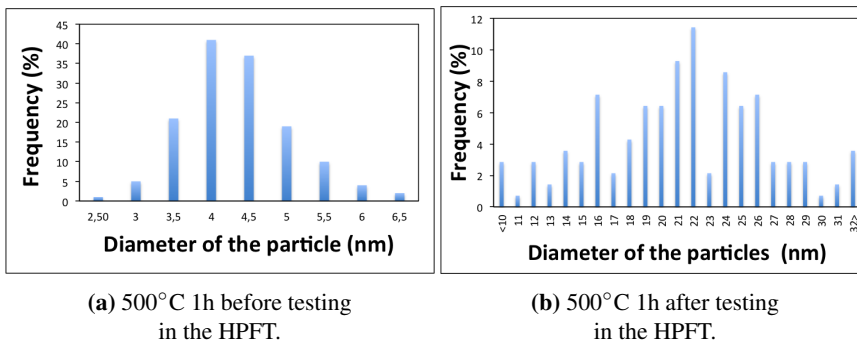
Figure 4.31: Particle distribution for 500°C 1h before and after testing in HPFT.

Particle size distribution for 500°C 1h before the testing in HPFT follow an approximately normal distributed curve and this is shown in Figure 4.31a. 55% of the particle size are in the diameter range 4-4.5 nm, shown from Figure 4.31a. For 500°C 1h before tested in FT 140 particles in the TEM pictures were measured. Particle size distribution for 500°C 1h after the testing in FT-rig are shown in Figure 4.31b. The particle sizes are much larger for 500°C 1h after the testing in HPFT, this shows to the particle grows together during the reaction. Most of the particles (45 %) are in the range 20-25 nm. The distribution shows that the diameters after the testing have been 4-5 times larger. 139 particles in the TEM pictures for 500°C 1h after testing were measured.

The particle size distribution for 600°C 1h are shown in Figures 4.32a and 4.32b. Figure 4.32a shows the particle size distribution before the reaction and Figure 4.32b shows after the reaction.
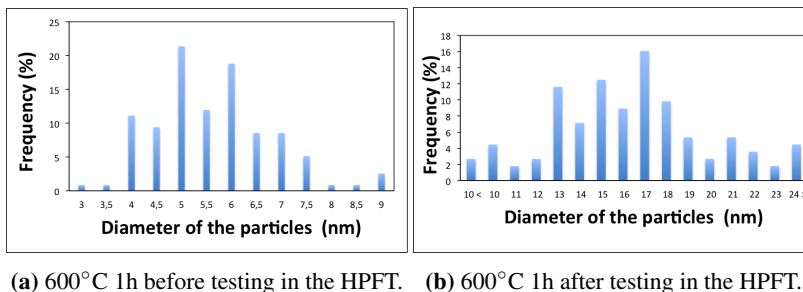
(a) 600°C 1h before testing in the HPFT.

(b) 600°C 1h after testing in the HPFT.

Figure 4.32: Particle distribution for 600°C 1h before and after testing in HPFT.

Catalyst 600°C 1h before testing at FT has largest particle size distribution of 5 and 6 nm diameter of the particles, this corresponds to 40 % of the particles size distribution, shown

in Figure 4.32a. 600°C 1h before testing also has high particle size distribution for 4, 4.5, 5.5, 6.5 and 7.0 nm. 600°C has a width range of particle size distribution because the range are from 3 to 9 nm. For 600°C 1h before tested in FT 117 particles in the TEM pictures were measured. 600°C 1h has larger particles than 500°C 1h before the testing. 600°C 1h after testing at FT has largest particle size distribution of 17 nm length of the particles and this corresponds to 16% of the particle distribution. 600°C 1h after testing at FT also has high particle size distribution for 13.0-18.0 nm, they corresponds to 66% of all the particle size distribution. 600°C 1h after testing at FT has width range from 10 to 24 nm. For 600°C 1h after testing 112 particles in the TEM pictures were measured.

The particle size distribution for 700°C 8h are shown in Figures 4.33a and 4.33b. Figure 4.33a shows the particle size distribution before the reaction and Figure 4.33b shows after the reaction.

(a) 700°C 8h before testing in the HPFT.   (b) 700°C 8h after testing in the HPFT.
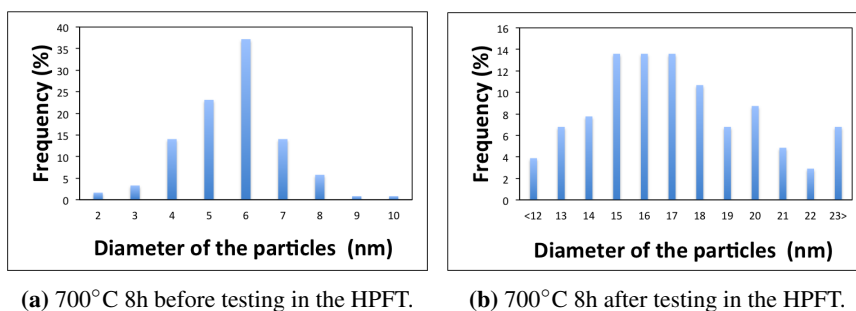
Figure 4.33: Particle distribution for 700°C 8h before and after testing in HPFT.

Particle size distribution for 700°C 8h before the testing in HPFT are follow a normal distribution curve and this is shown in Figure 4.33a. 700°C 8h before the testing in HPFT has largest particle size distribution for 6 nm and this corresponds to 37% of the particle size distribution. The amount of particles at 4 nm are equal to the amount of 7 nm (14 %). For 700°C 1h before tested in FT 121 particles in the TEM pictures were measured. Particle size distribution for 700°C 8h after the testing in FT has largest particles size distribution for 16.0-17.0 nm. There are also high distribution for 14.0-20.0 nm. 700°C 8h after the testing in FT has low distribution for particles larger than 22nm.For 700°C 8h after tested in FT 103 particles in the TEM pictures were measured. 700°C 8h after the testing in FT has smaller particles than 500°C 1h and 600°C 1h after HPFT.

Chapter 5

Discussion

The pyrolyzed samples have higher BET surface area than the ambient dried samples. The reason for smaller BET surface area for ambient dried samples are the pores are based on the dried biopolymer. During the pyrolyze the pores will be created from the former spaces from gases and liquids in the pyrolyze.

The BET surface area for 500°C 1h (460 m^2/g) is much larger than for 500°C 8h (298 m^2/g) . 500°C 1h have larger pore volume than 500°C 8h, but they have equal pore size. 500°C 1h and 500°C 8h are pyrolyzed at the same temperature, but the heating rate (5°C/min and 2°C/min) and hold time (1h and 8h) are difference, respectively. The difference in BET surface area and pore volume might be explained by the faster heating rate creates more gas and liquid. This result in more pores during the pyrolyze.

The BET surface area for 500°C 8h (393 m^2/g) is much larger than for 700°C 8h (298 m^2/g). 500° 8h have larger pore size than 700°C 8h, but they have same pore volume. The difference for BET surface area might be that the higher temperature creates more gases and liquids. This results in more pores during the pyrolyze.

Catalyst 400°C 1h and 500°C 1h reproduced was tested at both the degas temperature 80°C and 200°C. 400°C had approximately equal BET surface area, pore volume and pore size for both the degas temperatures. 500°C 1h reproduced increased the BET surface area from 157 m^2/g to 199 m^2/g when the degas temperature was changed from 80°C to 200°C. The 400°C 1h had very small BET surface area and pore volume. The low degas temperature was enough to remove almost all gas inside the catalyst material specimen. For 500°C 1h reproduced the BET surface area and the pore volume was much larger so the higher degas temperature removed more gas molecules.

The TGA analyze was carried out to demonstrate that the catalysts are thermal stable at temperatures above reduction reaction FTS (350°C). From mass loss as function of temperature the TGA results show small mass loss in the temperature range from 400-700°C.

The evaporation of the flue gases was constant in this temperature range. Therefore, the pyrolyze temperature range was 400-700°C. It was decided to pyrolyze catalysts at the following conditions: 400°C 1h, 500°C 1h, 600°C 1h, 500°C 8h and 700°C 8h.

High pressure FT test shows that 500°C 1h was a very active catalyst. The catalyst was at steady state at the high conversion 88 %. This catalyst was the first tested catalyst in the high pressure FT test. Therefore the mass of the catalyst was 0.5 g. It was decided to have 0.25 g mass of catalyst for all other catalysts for easier to adjust the GHSV.

Catalyst 500°C 1h has a very high BET surface area and high loading of iron. This might explain the very high activity registered during in the high pressure FT. 500°C 1h has smaller concentration of sodium and sulfur than the other pyrolyzed samples. The low concentration of sodium indicates the iron alginate beads were excellent washed in washing procedure during the preparation of the catalyst. In addition, the TEM pictures for 500°C 1h show the most finely distribution of the iron particles.

In the testing for 500°C 1h, the catalyst was tested with different flows. The flow in the beginning should be 225 ml/min, after 20 hours the flows was changed to 250 mL/min and then changed to 500 mL/min. Afterwards it was observed that the system was unsatisfactory calibrated. The flows were in fact 269, 299 and 598.6ml/min, respectively. A later check of the calibrations shows that 208.8 mL/min was 250 mL/min. The flow for the other catalysts were 250 mL/min. The flow for the other catalysts were reduced by the half for steady state.

Catalyst 600°C 1h was also an active catalyst (86 %), but the catalyst deactivated immediately after the highest conversion was reached. 600°C 1h has a high BET surface area (316 m^2/g), high loading of iron, low concentration of sodium and sulfur. The TEM pictures shows finely distribution of iron particles. Then, the 600°C 1h is supposed to have potential to achieve the same FT activity as 500°C 1h. The BET surface area for 600°C 1h is somewhat smaller than for 500°C 1h. They have approximately equal pore volume and pore size. It would be very interesting to test the 600°C 1h for longer time to see steady state areas for 600°C 1h.

Catalyst 700°C 8h was the catalyst with highest conversion (92 %), but this catalyst also deactivated immediately after the highest conversion. 700°C 8h has a very high BET surface area (393 m^2/g), high loading of iron, low concentration of sulfur. 700°C 8h has higher concentration of sodium than the other pyrolyzed samples.

500°C 1h reproduced was a medium active catalyst with the highest conversion (65 %), but immediately decreased after the maximum conversion. 500°C 1h reproduced has a low BET surface area (157 m^2/g). 500°C 1h reproduced has smaller pore volume than the other pyrolyzed samples. 500°C 1h reproduced has much lower loading of iron than the other pyrolyzed samples. The concentration of sodium is much higher than the other pyrolyzed samples. Compared with 500°C 1h original, the 500°C 1h reproduced has 3 times higher concentration of sodium. This indicate the iron alginate beads were not suf-

ficient washed. 500°C 1h reproduced had approximately equal concentration of sulfur. Catalyst 500°C 1h reproduced had also smaller surface area than the original 500°C 1h.

500°C 1h and 500°C 1h reproduced were the only produced catalyst which obtained steady state. 500°C 1h reproduced should have been tested during longer time at HPFT because the catalyst was stable from 25 to 40 hours. The testing was stopped because the gas bottle for syngas was empty.

Catalyst 400°C 1h has very small BET surface area, the loading of iron is much smaller than the other pyrolyzed samples. 400°C 1h has the highest concentration of sodium of all the pyrolyzed samples. The high concentration of sodium indicates the iron alginate beads were not sufficiently washed. 400°C 1h has the lowest concentration of sulfur. This can be the reason for the very low CO conversion from the HPFT testing. The low pyrolyze temperature can also have a negative effect for the low conversion. 400 °C is the lowest possible pyrolyze temperature shown from TGA results. At 400°C the mass % does continue decrease. The change in mass % is due to combustion of flue gases. Therefore, catalysts pyrolyzed at temperatures lower than 400°C are not considered sufficient thermal stability for use in the Fischer- Tropsch.

Catalyst 500°C 8h was also tested at the high pressure FT. Leakage in the HPFT-rig occurred during this test and destroyed the sample. The test results from 500°C 8h would be very much appreciated. They would give a completed serie of all the pyrolyzed samples tested in HPFT. 500°C 8h has high surface area, high loading of iron and low concentration of sodium. These properties are supposed to give high CO conversion in the HPFT test.

For all the catalyst tested with high pressure FT, the testing started when the temperature was 340°C, the pressure was 20 bar and the syngas was introduced. The first measurement will report when the syngas reacts with the catalyst. It takes some time to fill the system with syngas and depress all helium. If the syngas introduces before the test starts, the syngas may interact with the catalyst before the testing. The result will be a deactivated catalyst. The reason for comparing of 500°C 1h at GHSV 71 839 and the other catalysts at 60 000 is that the GHSV value is of the same order of magnitude. The higher GHSV for the 500°C 1h was because the higher flow and more mass of catalyst. The conversion for 500°C 1h was selected to 67 % because the catalyst was at steady state and GHSV 71 839. For the catalysts 600°C 1h, 500°C 1h reproduced and 700°C 8h GHSV 60 000 and conversions most equal to 67% were selected. 400°C 1h had very low conversion with a highest value of 26%. This low value of conversion (26%) at GHSV 60 000 was selected to compare with the other catalysts. The reference had also low conversion, the highest conversion (42%) at GHSV 60 000 was selected.

The calculations for GHSV and FTY in HPFT were adjusted with iron loading from ICP-MS because this is the most precise iron loading. Conditions which have effect for the GHSV are the flow and mass of the catalysts. Conditions which have effect for the FTY are the CO conversion, flow of CO, selectivity of CO_2 and mass of catalysts.

Catalysts 500°C 1h, 500°C 8h, 600 °C and 700 °C 8h were produced from distilled water for the alginate production. Deionized water was used for alginate production for 500°C reproduced and 400°C. The reason for using distilled in stead of deionized water was more pure water. Use of deionized water was to avoid undesired ions in the samples. It was reported about problem with the reliability of the equipment for production of deionized water at the laboratory. This might explain the lower performance for 500°C 1h reproduced and 400°C 1h.

Only 500°C 8h and 700°C 8h were tested in the low pressure FT test because problems with the equipment. The product distribution shows carbon selectivity (%) within hydrocarbon products. The equipment was not satisfactory calibrated to obtain reliable data for CO_2. It is not possible to compare the activity and the selectivity for LPFT and HPFT because only the catalyst 500°C 8h was tested for both LPFT and HPFT.

All the samples have a small concentration of sulfur. The source of sulfur is the alginate. The pyrolyzed samples have higher concentration of sulfur than ambient dried samples. This is because some of the carbon is combusted during the pyrolyze and the total mass decreased.

Calculations for theoretical loading of iron is based on two alginate monomers reacts with one Fe-ion. Fe^{3+} is 3 valent, but it is only space for two monomers of alginate to react with one iron ion. Accessible for active sites at the iron-ions for the alginate monomers will depend on the amount of bonded iron alginates. Amount of bonded iron alginates will also depend on the accessible G or M units, this because G-units follows to cross-linking of the hydrogel.

The iron loading calculated from TGA and the ICP-MS results approximately follows the same trends. ICP-MS ICP-MS is a more precise analyzing method because this type of analyzing is based on measured exited and emitted ions in the samples. TGA is only based on measuring the weight before the testing and then measure the amount of flue gas during the reaction. Therefore, ICP-MS are used for the FT- calculations.

S(T)EM technique is very helpful for characterization and determination of elements (including distribution) at a very low scale (at "nano" level). The results might be valuable to obtain understanding of particle size, shape, distribution, composition, etc. All materials and samples have inhomogeneities. Therefore, the results from S(T)EM analysis may not be generalized and concluded as representative for the whole sample/specimen examined. Increased number of S(T)EM samples will increase the confidence about general behavior. However, in most cases, S(T)EM is valuable to give supporting information about behavior at "nano" level.

The reference catalyst should also have been analyzed with ICP-MS, but it was agreed at an early stage that this should not be focused in this task. Therefore, the HPFT calculations for the reference catalyst are based on iron loading from the suppliers (Clariant).

Based on the testing of the produced catalyst the reference catalyst had low conversion (41 %), but the reference catalyst was obtained steady state from 14 hours. The reference catalyst has much higher carbon selectivity of CH_4 than the produced catalyst. It is not possible to give further explanation about the low conversion and the selectivity of the reference catalyst because the reference catalyst was not characterized.

All the produced catalysts tested in HPFT have lower carbon selectivity of CH_4 than the reference catalyst. CH_4 is an undesired product. This means the produced catalysts are better than the reference catalyst.

TEM pictures for the particles before high pressure FT test shows mainly spherical particles. The TEM pictures for the particles after the high pressure FT test shows both spherical and rectangular shaped particles. For the rectangular shaped particles the shortest side were measured. It was measured 100-140 particles per TEM pictures.

The TEM pictures shows the most finely distributed particles for catalyst 500°C 1h. The TEM pictures for 700°C 8h shows larger particles and some of the iron particles are grown together. The reason for the sintering of the particles might be the very high temperature. The TGA results in argon shows decreasing in mass in the temperature range 600-700°C. This might be an indication that 700°C is close to an upper temperature for thermal stability of the catalysts produced.

It was decided that the task should select to pyrolyze large batches of 20 wt% alginate solutions. The results from the test series with 20 wt% are presented in this report. The BET surface area shows larger surface area for 10 and 15 wt% alginate solution. Therefore, for comparison results from similar test series with lower concentrations might be interesting.

The concentration of sodium and sulfur in addition to TEM pictures before and after testing are not sufficient to describe the deactivation of the catalysts. The amount of iron carbide will describe the hight of the activity of the iron. The iron particles can oxidize during the FTS. In situ technique as Mossbauer can give oxidation state of iron. This technique was not accessible for this work.

The experimental work shows that Sodium and Sulphur have some effect, and mostly negative. A unfavorable "higher" level of sodium in the specimen might come from the washing and a possible source might be the deionized water used. The Sulphur might come from natural presence in the alginate, and hence more difficult to avoid. It might be an advantage to better understand the effect of these elements and do supporting tests with catalyst only study these effects. This is supposed to be interesting for further optimizing the washing prior to pyrolyze and hence obtain catalysts with better performance.

The results from the experimental work in this task including comparison of data from the characterization the following is considered essential to obtain an alginate reliable catalyst with good performance. Preparation and proper washing is important to ensure low

impurity level. High BET surface area and pore volume, pyrolyze conditions and finely distribution of particles from TEM pictures are important factors to obtain catalysts with good performance. All the produced and tested catalyst in this task show smaller methane selectivity than the reference catalyst. The reference catalyst has not been characterized in this experimental work,the data is based on information from the supplier. Even though the good results reported it might be an advantage, both with respect to better understanding and increased the confidence to obtain results from repeated same test conditions. In addition, some parameters should be changed.

Chapter 6

Conclusion

Iron is a catalyst for FTS. A weakness of iron as catalyst for FTS is the poor mechanic stability at high temperatures. The iron particles interact with the syngas and this results in formation of iron carbides. Alginate was used as biopolymer to get a better distribution of the iron particles. Alginate was produced in five different concentrations (2.5, 5.0, 10, 15 and 20 wt%). Iron nitrate ($Fe(NO_3)$ 0.1 M) were dissolved in alginate and made iron-alginate-beads. Large batches of 20 wt% were pyrolyzed at the conditions: 400°C 1h, 500°C 1h, 500°C 1h reproduced, 600°C 1h, 500°C 8h and 700°C 8h. The catalysts were characterized with BET, TGA, ICP-MS, XRD, TEM and S(T)EM.

TGA and ICP-MS results shows high loading of iron 20-30 wt% for pyrolyzed catalyst. The TGA and ICP-MS result shows loading of iron for the ambient dried samples to be 3-13 wt%. The BET surface area for the ambient dried samples were 141, 237, 271, 259 and 255 m^2/g for 2.5, 5.0, 10.0, 15.0 and 20 wt%. BET surface area for pyrolyzed samples were 22.2, 460, 157, 316, 298 and 393 m^2/g for 400°C 1h, 500°C 1h, 500°C 1h reproduced, 600°C 1h, 500°C 8h and 700°C 8h, respectively.

The catalysts 500°C 8h and 700°C 8h were tested in LPFT. The conversion of 500°C 8h were 5.0 % and 10.0 % at the flow ratios (H_2:CO) 1:1 and 10:1, respectively. The conversion of 700°C 8h was 8.0%. The carbon selectivity within hydrocarbon products for 500°C 8h shows highest production of C5+ for both 1:1 and 10:1. The carbon selectivity within hydrocarbon products for 700°C 8h shows highest distribution of $C_2 - C_4$ total olefins.

The catalysts 400°C 1h, 500°C 1h, 500°C 1h reproduced, 600°C 1h, 700°C 8h and the reference catalyst were tested in HPFT. 500°C 1h was a very active catalyst and was stable at the conversions 88% and 67%. 600°C 1h and 700°C 8h obtained the high conversions 86% and 92%, respectively. 600°C 1h and 700°C 8h immediately deactivated after the highest conversions. 500°C 1h reproduced obtained the highest conversion 65%. 500°C 1h reproduced immediately deactivated to steady state range 34%. 400°C 1h had very low

conversion and obtained the highest conversion 26%. The reference catalyst was steady state at 41% and 71%.

The catalysts were compared at GHSV 60 000 $cm^3/gmin$ and conversion 65%. The FTY at this comparison were 5.1· 10^{-4} , 5.2· 10^{-4} , 7.2· 10^{-4} , 4.0· 10^{-4} and 4.4) · 10^{-4} $molCO/g_{Fe}s$ for the catalysts 400°C 1h, 500°C 1h, 500°C 1h reproduced, 600°C 1h and 700°C 8h, respectively. The FTY for the reference catalyst was $7.9 \cdot 10^{-5} \ molCO/g_{Fe}s$. All the catalysts tested at HPFT had highest carbon selectivity within hydrocarbons of C5+. All the produced catalyst had smaller carbon selectivity of CH_4 than the reference catalysts.

Catalyst 500°C 1h had the best performance among those tested. 500°C 1h had the best particle distribution from TEM, highest BET surface area, high loading of iron and low concentrations of sodium and sulfur. The experimental work shows that the best performance are obtained in a catalyst with the following behavior: pyrolyze conditions, high iron loading, even and fine grained particle distribution and large BET surface area.

Chapter 7

Future Work

The reported work has shown catalysts with good performance and to a large extent also highlighted important factors for production of catalysts. In some cases, the experimental work had too few parallels to make a firm conclusion. The discussion chapter has also highlighted some need for supporting analysis and additional tests with same and/or various test condition to establish higher confidence.

The following are recommended for further work to establish a better data base:

- BET surface area, pore structure and pore volume analysis should be repeated to verify the results.

- Catalyst 20 wt% pyrolyzed 500°C 1h should be reproduced one more time. Distilled water for the alginate solution should be used because the original 20 wt% pyrolyzed 500°C 1h was based on distilled water. Hopefully, this new reproduced catalysts also will have the same very large BET surface area (460 m^2/g). Hopefully, this new catalyst also will get very high conversion and steady-state range as the original 20 wt% pyrolyzed 500°C 1h. 20 wt% pyrolyzed 400°C 1h should also be reproduced using distilled water. It would be interesting to see if this will give same trends with very low BET surface area, small pore volume and large pore sizes, and very low conversion in the testing of HPFT.

- New calibration of CO_2 in the system for low pressure FT will give better basis for the testing in LPFT. With better a calibrated system for CO_2, the product distribution for LPFT will be CO_2, CH_4, $C_2 - C_4$ total olefins, $C_2 - C_4$ total parafins and C5+. All the pyrolyzed catalyst and the reference catalyst should be tested in the LPFT. Completed series of all the catalysts will give a better base for the comparison for the activity and selectivity for the catalyst tested at LPFT.

- 20 wt% pyrolyzed 500°C 8h should also be tested at HPFT. This will give a completed serie of all the catalyst tested HPFT. Completed testing of all the catalyst at HPFT and LPFT will give an excellent basis for comparison of the catalysts at high and low pressure FT.

- Catalysts with 15 wt% alginate solution should be produced and pyrolyzed at same temperatures and dwelling time as 20 wt%. Characterization and testing should be as for those tested in this work.

Bibliography

[1] Aylaward G. and Findlay Tristan, *SI Chemical Data 6th edition*. Milton: John Wiley and Sons Australia, 2008.

[2] Yang Jia, "A steady-state isotopic traninsent kinetic study of cobolt catalysts: Mechanistic insights and effect of cobalt particle size, supports and promoters."

[3] N. J. Chorkendorff I., *Concepts of Modern Catalysis and Kinetics, second Revisted and Enlarged Edition,*.

[4] Agulhon, Pierre et. all. , "Controlled synthesis from alginate gels of cobalt-managanese mixed oxide nanocrystals with peculiar magnetic properties." `http://www.sciencedirect.com/science/article/pii/S0920586112002180`. [Visited on 2017-10-10].

[5] Steynberg A. P. , "Studies in surface science and catalysis, chapter 1 - introduction to fischer-tropsch technology."

[6] Dry Mark E. , "The fischer–tropsch process: 1950–2000." `https://www.sciencedirect.com/science/article/pii/S0920586101004539`. [Visited on 2018-05-21].

[7] Olewski T et all, "Hydrocarbon selectivity models for iron-based fischer–tropsch catalyst." `https://www.sciencedirect.com/science/article/pii/S026387621500009X`. [Visited on 2018-05-21].

[8] Todic B., Nowicki L., Nikacevic N., Bukur D. B. , "Fischer–tropsch synthesis product selectivity over an industrial iron-based catalyst: Effect of process conditions."

[9] Shell, "Pearl gtl overview." `https://www.shell.com/about-us/major-projects/pearl-gtl/pearl-gtl-an-overview.html`. [Visited on 2018-05-21].

[10] Liu Guoguo et all, "Nitrogen-rich mesoporous carbon supported iron catalyst with superior activity for Fischer-Tropsch synthesis." `https://www.`

sciencedirect.com/science/article/pii/S0008622318300150. [Visited on 2018-06-17].

[11] Xie, Jingxiu , "Catalyst Design and Development for the Direct Production of Lower Olefins from Synthesis Gas."

[12] Maitlis Peter M. Klerk Arno de , "Greener Fischer-Tropsess Processess for Fuels and Feedstocks, John Wiley & Sons." http://ebookcentral.proquest.com/lib/ntnu/reader.action?docID=1120964&ppg=1. [Visited on 2017-12-16].

[13] Santos Vera P. et all, "Metal organic framework-mediated synthesis of highly active and stable Fischer-Tropsch catalyst." https://www.nature.com/articles/ncomms7451. [Visited on 2018-04-24].

[14] Bukur, Dragomir B., Elbashir Nimir, "Role of water-gas-shift reaction in Fischer–Tropsch synthesis on iron catalysts: A review." http://www.sciencedirect.com/science/article/pii/S0920586115007233. [visited on 2017-12-16].

[15] Botes Gideon F. et. al , "Development of a chemical selective iron Fischer Tropsch catalyst." http://www.sciencedirect.com/science/article/pii/S0920586115007920. [Visited on 2017-12-16].

[16] Dry, M. E., "Present and future applications of the Fischer-Tropsch process. Applied Catalysis a general." https://www.researchgate.net/publication/257372847_Present_and_future_applications_of_the_Fischer-Tropsch_process. [Visited on 2017-12-16].

[17] Ding, Mingyue et. all , "Study on reduction and carburization behaviors of iron phases for iron-based Fischer–Tropsch synthesis catalyst." https://www.sciencedirect.com/science/article/pii/S0306261914012999. Visited on 2017-12-16].

[18] Li Jifan et all, "Effect of alkalis on iron-based Fischer-Tropsch synthesis catalysts: Alkali-FeOx interaction, reduction, and catalytic performance." https://www.sciencedirect.com/science/article/pii/S0926860X16304987. [Visited on 2018-06-17].

[19] Rowley, Jon A. Madlambayan Gerard, Mooney David J., "Alginate hydrogels as synthetic extracellular matrix materials." https://ac.els-cdn.com/S0142961298001070/1-s2.0-S0142961298001070-main.pdf?_tid=44bb9d58-ada0-11e7-b279-00000aacb35d&acdnat=1507629132_7978d92cc8d61722578a4dc63ae60da6. [Visited on 2017-10-10].

[20] Guibal Eric, Vincent Thierry, Blondet Francisco Peirano , "Biopolymers as Supports for Heterogeneous Catalysis: Focus on Chitosan, a Promising Aminopolysaccharide."

[21] Condon, James B., "Sureface Area and porosity Determinations by Physisorption, Measurements and Therory." `http://files.instrument.com.cn/bbs/upfile/files/20120206/20122618358.pdf`. [Visited on 2017-10-10].

[22] Bruanuer, Stephen, Emmett, P. H. and Teller Edward, "Adsorption of Gases in Multimolecular Lauers." `http://pubs.acs.org/doi/pdf/10.1021/ja01269a023`. [Visited on 2017-12-13].

[23] Legras A. et al, "Inverse gas chromatography for natural fibre characterisation: Identification of the critical parameters to determine the Brunauer–Emmett–Teller specific surface area, Journal of Chroatography A." `https://www.sciencedirect.com/science/article/pii/S0021967315016611`. [Visited on 2017-12-13].

[24] Agrawal, Ankit and Chakraborty, "A kinetic study of pyrolysis and combustion of microalgae Chlorella vulgaris using thermo-gravimetric analysis." `http://www.sciencedirect.com/science/article/pii/S0960852412015453`. [Visited on 2017-09-06].

[25] Selbekk, Rune S. , "Termogravimetri." `https://snl.no/termogravimetri`. [Visited on 2017-12-13].

[26] Li Qingzhao , "Comparison of pulverized coal combustion in air and in O2/CO2 mixtures by thermo-gravimetric analysis, Journal of Analytical and Applied Pyrolysis." `http://www.sciencedirect.com/science/article/pii/S0165237008001459`. [Visited on 2017-09-05].

[27] Jenner G.A et all, "ICP-MS — A powerful tool for high-precision trace-element analysis in Earth sciences: Evidence from analysis of selected U.S.G.S. reference samples." `https://www.sciencedirect.com/science/article/pii/000925419090145W`. [Visited on 2018-04-26].

[28] Taylor Howard E., *Inductively Coupled Plasma-Mass Spectrometry : Practices and Techniques*. Weinheim: San Diego : Academic, 2001.

[29] Egelanf Einar Skarstad, "ICP." `https://snl.no/ICP`. [Visited on 2018-04-26].

[30] Dutrow Barabara, Clark Christine M, "X-ray Powder Diffraction (XRD)." `https://serc.carleton.edu/research_education/geochemsheets/techniques/XRD.html`. [Visited on 2017-12-17].

[31] Myronyuk, Ivan F., "Structural Features of Carbons Produced Using Glucose, Lactose, and Saccharose." `https://www.ncbi.nlm.nih.gov/pmc/articles/PMC5114214/`. [Visited on 2018-12-13].

[32] Britannica academic, "Electron microscopy." `http://academic.eb.com/levels/collegiate/article/electron-microscopy/472263`. [Visited on 2017-11-06].

[33] J. W. Niemantsverdriet, *Spectroscopy in Catalysis: An Introduction, Third Edition.* Weinheim: WILEY-VCH Verlag GmbH Co. KGaA, 2007.

[34] Wang Z. L, "Transmission Electron Microscopy of Shape-Controlled Nanocrystals and Their Assemblies." `http://pubs.acs.org/doi/full/10.1021/jp993593c`. [Visited on 2017-11-11].

[35] Fogler H. Scott, *Essentials of chemical reaction engineering* . United States of America: Pearson Education, 2011.

[36] Ledesma C. Yang J. Chen D. and Holmen Anders, "Recent Approaches in Mechanistic and Kinetic Studies of Catalytic Reactions Using SSITKA Technique." `https://pubs.acs.org/doi/full/10.1021/cs501264f`. [Visited on 2018-04-25].

[37] Clariant, "Syngas catalysts create performance technology® for syngas processes." `https://www.clariant.com/en/Business-Units/Catalysts/Chemical-Catalysts`. [Visited on 2018-06-17].

[38] Jia Yang, "Personal communication."

Appendix A

HSE Risk Assessment

This appendix is the risk assessment for the experimental work

			Status	**Dato**
ID	22622		Opprettet	14.09.2017
Risikoområde	Risikovurdering: Helse, miljø og sikkerhet (HMS)		Vurdering startet	14.09.2017
Opprettet av	Marit Liebe Harneshaug		Tiltak besluttet	
Ansvarlig	Marit Liebe Harneshaug		Avsluttet	

Risikovurdering:
Synthesis, characterization and catalytic testing of Iron-Alginte catalysts

Gyldig i perioden:
-

Sted:
Laboratories in K5 and Chemistry Hall

Mål / hensikt
Risk assessment of catalyst preparation and testing.

Bakgrunn
Preparation of iron alginate hydrogels, followed by drying and calcination.
Charactereization of the catalyst with TGA, XRD,XRF, BET, SEM, TEM and STEM
Catalytic testing in Fischer-Tropsch rig.

Beskrivelse og avgrensninger
Weighing and mixing of alginate, water and iron-precursors.
Solvent-exchange of water with ethanol.
Drying and calcination of the gel.
Catalytic testing in Fischer-Tropsch rig

Forutsetninger, antakelser og forenklinger
[Ingen registreringer]

Vedlegg
[Ingen registreringer]

Referanser
[Ingen registreringer]

Oppsummering, resultat og endelig vurdering

I oppsummeringen presenteres en oversikt over farer og uønskede hendelser, samt resultat for det enkelte konsekvensområdet.

Farekilde:	**Synthesis of iron alginate gel**

Uønsket hendelse:	**Chemical burns**

Konsekvensområde: Helse   Risiko før tiltak: 🟢 Risiko etter tiltak: ⚪

Farekilde:	**Solvent-exchange**

Uønsket hendelse:	**Ignition of ethanol**

Konsekvensområde: Helse   Risiko før tiltak: 🟢 Risiko etter tiltak: ⚪

Farekilde:	**Drying**

Uønsket hendelse:	**Burns**

Konsekvensområde: Helse   Risiko før tiltak: 🟢 Risiko etter tiltak: ⚪

Farekilde:	**Calcination**

Uønsket hendelse:	**Burns**

Konsekvensområde: Helse   Risiko før tiltak: 🟢 Risiko etter tiltak: ⚪

Farekilde:	**XRD**

Uønsket hendelse:	**Exposure to calcined powder**

Konsekvensområde: Helse   Risiko før tiltak: 🟢 Risiko etter tiltak: ⚪

Farekilde:	**TGA**

Uønsket hendelse:	**Burns**

Konsekvensområde: Helse   Risiko før tiltak: 🟢 Risiko etter tiltak: ⚪

Farekilde:	**XRF**

Uønsket hendelse:	**Exposure to radiation**

Konsekvensområde: Helse   Risiko før tiltak: 🟢 Risiko etter tiltak: ⚪

Farekilde:	**BET**

Uønsket hendelse:	**Frostbite from liquid nitrogen**

Konsekvensområde: Helse   Risiko før tiltak: 🟢 Risiko etter tiltak: ⚪

Farekilde:	**Fischer- Tropsch Synthesis**

Uønsket hendelse:	**Gas leak**

Konsekvensområde: Helse   Risiko før tiltak: 🟡 Risiko etter tiltak: ⚪
Materielle verdier   Risiko før tiltak: 🟢 Risiko etter tiltak: ⚪

Uønsket hendelse:	**Burns**

Konsekvensområde: Helse   Risiko før tiltak: 🟢 Risiko etter tiltak: ⚪
Materielle verdier   Risiko før tiltak: 🟢 Risiko etter tiltak: ⚪

Farekilde:	**Supercritical drying**

Uønsket hendelse:	**Spill of acetone**

Konsekvensområde: Helse   Risiko før tiltak: 🟢 Risiko etter tiltak: ⚪
Materielle verdier   Risiko før tiltak: 🟢 Risiko etter tiltak: ⚪

Uønsket hendelse:	**leak of CO2**

Konsekvensområde: Helse   Risiko før tiltak: 🟢 Risiko etter tiltak: ⚪
Materielle verdier   Risiko før tiltak: 🟢 Risiko etter tiltak: ⚪

Endelig vurdering

Involverte enheter og personer

En risikovurdering kan gjelde for en, eller flere enheter i organisasjonen. Denne oversikten presenterer involverte enheter og personell for gjeldende risikovurdering.

Enhet /-er risikovurderingen omfatter

- Institutt for kjemisk prosessteknologi

Deltakere

Jia Yang

Joakim Tafjord

Lesere

Karin Wiggen Dragsten

Gunn Torill Wikdahl

Andre involverte/interessenter

[Ingen registreringer]

Følgende akseptkriterier er besluttet for risikoområdet Risikovurdering: Helse, miljø og sikkerhet (HMS):

Helse	Materielle verdier	Omdømme	Ytre miljø

Oversikt over eksisterende, relevante tiltak som er hensyntatt i risikovurderingen

I tabellen under presenteres eksisterende tiltak som er hensyntatt ved vurdering av sannsynlighet og konsekvens for aktuelle uønskede hendelser.

Farekilde	Uønsket hendelse	Tiltak hensyntatt ved vurdering
Synthesis of iron alginate gel	Chemical burns	laboratory coat
	Chemical burns	Goggles
Solvent-exchange	Ignition of ethanol	laboratory coat
	Ignition of ethanol	Fume hood
	Ignition of ethanol	Laboratory training
	Ignition of ethanol	Chemical safety data sheets
	Ignition of ethanol	Goggles
Drying	Burns	laboratory coat
	Burns	Gloves
	Burns	Equipment training
	Burns	Laboratory training
	Burns	Goggles
Calcination	Burns	laboratory coat
	Burns	Fume hood
	Burns	Equipment training
	Burns	Laboratory training
	Burns	Goggles
XRD	Exposure to calcined powder	Gloves
	Exposure to calcined powder	Equipment training
	Exposure to calcined powder	Laboratory training
	Exposure to calcined powder	Chemical safety data sheets
	Exposure to calcined powder	Goggles
TGA	Burns	laboratory coat
	Burns	Gloves
	Burns	Fire extinguisher
	Burns	Equipment training
	Burns	Laboratory training
	Burns	Chemical safety data sheets
	Burns	Goggles
XRF	Exposure to radiation	Equipment training
	Exposure to radiation	Laboratory training
BET	Frostbite from liquid nitrogen	laboratory coat
	Frostbite from liquid nitrogen	Gloves

BET	Frostbite from liquid nitrogen	Equipment training
	Frostbite from liquid nitrogen	Laboratory training
	Frostbite from liquid nitrogen	Goggles
Fischer- Tropsch Synthesis	Gas leak	laboratory coat
	Gas leak	Fire extinguisher
	Gas leak	Equipment training
	Gas leak	Laboratory training
	Gas leak	Chemical safety data sheets
	Gas leak	Gas alarm
	Gas leak	Goggles
	Burns	laboratory coat
	Burns	Fire extinguisher
	Burns	Equipment training
	Burns	Laboratory training
	Burns	Chemical safety data sheets
	Burns	Gas alarm
	Burns	Goggles
Supercritical drying	Spill of acetone	laboratory coat
	Spill of acetone	Equipment training
	Spill of acetone	Laboratory training
	Spill of acetone	Goggles
	leak of CO2	Equipment training
	leak of CO2	Laboratory training
	leak of CO2	Chemical safety data sheets
	leak of CO2	Gas alarm

Eksisterende og relevante tiltak med beskrivelse:

laboratory coat
[Ingen registreringer]

Fume hood
[Ingen registreringer]

Gloves
[Ingen registreringer]

Working alone alarm
[Ingen registreringer]

Fire extinguisher
[Ingen registreringer]

Equipment training
[Ingen registreringer]

Laboratory training
[Ingen registreringer]

Chemical safety data sheets
[Ingen registreringer]

Gas alarm
[Ingen registreringer]

Goggles
[Ingen registreringer]

Risikoanalyse med vurdering av sannsynlighet og konsekvens

I denne delen av rapporten presenteres detaljer dokumentasjon av de farer, uønskede hendelser og årsaker som er vurdert. Innledningsvis oppsummeres farer med tilhørende uønskede hendelser som er tatt med i vurderingen.

Følgende farer og uønskede hendelser er vurdert i denne risikovurderingen:

- **Synthesis of iron alginate gel**
  - Chemical burns
- **Solvent-exchange**
  - Ignition of ethanol
- **Drying**
  - Burns
- **Calcination**
  - Burns
- **XRD**
  - Exposure to calcined powder
- **TGA**
  - Burns
- **XRF**
  - Exposure to radiation
- **BET**
  - Frostbite from liquid nitrogen
- **Fischer- Tropsch Synthesis**
  - Gas leak
  - Burns
- **Supercritical drying**
  - Spill of acetone
  - leak of CO2

Detaljert oversikt over farekilder og uønskede hendelser:

Farekilde: Synthesis of iron alginate gel

Uønsket hendelse: Chemical burns

Sannsynlighet for hendelsen (felles for alle konsekvensområder):   **Lite sannsynlig (2)**

     Kommentar:

     High stirring speeds will not be used, and care will be taken when treating this solution.

Konsekvensområde: Helse   *Risiko:*

     Vurdert konsekvens: **Liten (1)**

          Kommentar: [Ingen registreringer]

Farekilde: Solvent-exchange

Uønsket hendelse: Ignition of ethanol

Sannsynlighet for hendelsen (felles for alle konsekvensområder): **Svært lite sannsynlig (1)**

Kommentar:

No sparks or flames will be present when using ethanol. Ethanol will be treated in a fume hood.

Konsekvensområde: Helse

Risiko:

Vurdert konsekvens: **Middels (2)**

Kommentar: [Ingen registreringer]

Farekilde: Drying

Uønsket hendelse: Burns

Årsak: Not using gloves or laboratory coat

Sannsynlighet for hendelsen (felles for alle konsekvensområder): **Lite sannsynlig (2)**

Kommentar:

Heat resistant gloves will be used when removing glass-ware from the furnace.

Konsekvensområde: Helse   *Risiko:*

Vurdert konsekvens: **Middels (2)**

Kommentar: [Ingen registreringer]

Farekilde: Calcination

Uønsket hendelse: Burns

Sannsynlighet for hendelsen (felles for alle konsekvensområder):   **Svært lite sannsynlig (1)**

      Kommentar:

      [Ingen registreringer]

Konsekvensområde: Helse   *Risiko:*

     Vurdert konsekvens: **Middels (2)**

       Kommentar: [Ingen registreringer]

Farekilde: XRD

Uønsket hendelse: Exposure to calcined powder

Sannsynlighet for hendelsen (felles for alle konsekvensområder):   **Svært lite sannsynlig (1)**

> *Kommentar:*
> [Ingen registreringer]

Konsekvensområde: Helse

> *Vurdert konsekvens:* **Liten (1)**
>
> *Kommentar:* [Ingen registreringer]

Risiko:

Farekilde: TGA

Uønsket hendelse: Burns

Årsak: touching very hot equipment

Sannsynlighet for hendelsen (felles for alle konsekvensområder):   **Svært lite sannsynlig (1)**

> *Kommentar:*
> [Ingen registreringer]

Konsekvensområde: Helse   *Risiko:*

> *Vurdert konsekvens:* **Middels (2)**
>
> > *Kommentar:* Vil i værste fall kunne få moderate brannskader.

Farekilde: XRF

Uønsket hendelse: Exposure to radiation

Årsak: Radiation

Sannsynlighet for hendelsen (felles for alle konsekvensområder):   **Svært lite sannsynlig (1)**

Kommentar:
[Ingen registreringer]

Konsekvensområde: Helse   *Risiko:*

Vurdert konsekvens: **Middels (2)**

Kommentar: [Ingen registreringer]

Farekilde: BET

Uønsket hendelse: Frostbite from liquid nitrogen

Årsak: Ved påsetting av prøvene i BET

Beskrivelse:
Frostskade på hender, armer eller sprut opp i ansiktet

Årsak: Ved fylling av flytende nitrogen

Beskrivelse:
ved påfylling av flytende nitrogen på kjemihall 1.etage.

Sannsynlighet for hendelsen (felles for alle konsekvensområder): **Lite sannsynlig (2)**

Kommentar:
[Ingen registreringer]

Konsekvensområde: Helse

Risiko:

Vurdert konsekvens: **Middels (2)**

Kommentar: [Ingen registreringer]

Norges teknisk-naturvitenskapelige universitet (NTNU)

Unntatt offentlighet jf. Offentlighetsloven § 14

Utskriftsdato:

11.12.2017

Utskrift foretatt av:

Marit Liebe Harneshaug

Side:

16/22

Farekilde: Fischer- Tropsch Synthesis

Uønsket hendelse: Gas leak

- -

Årsak: gas leak

Sannsynlighet for hendelsen (felles for alle konsekvensområder): **Svært lite sannsynlig (1)**

> *Kommentar:*
> Alle ventiler på rig´n vil bli testet før gass tilføres. Ventilene testes i fast prosedyre og testingen gjøres med såpevann. Det er montert gas detektorer på rig´n. Gassalarmen detekterer i to trinn. En høy gass alarm og en lav gassalarm.

Konsekvensområde: Helse

Vurdert konsekvens: **Stor (3)**

> *Kommentar:* [Ingen registreringer]

Risiko:

Konsekvensområde: Materielle verdier

Vurdert konsekvens: **Middels (2)**

> *Kommentar:* [Ingen registreringer]

Risiko:

Uønsket hendelse: Burns

- -

Sannsynlighet for hendelsen (felles for alle konsekvensområder): **Svært lite sannsynlig (1)**

> *Kommentar:*
> [Ingen registreringer]

Konsekvensområde: Helse

Vurdert konsekvens: **Middels (2)**

> *Kommentar:* [Ingen registreringer]

Risiko:

Norges teknisk-naturvitenskapelige universitet (NTNU)

Unntatt offentlighet jf. Offentlighetsloven § 14

Utskriftsdato:

11.12.2017

Utskrift foretatt av:

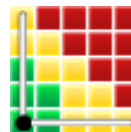Marit Liebe Harneshaug

Side:

17/22

Konsekvensområde: Materielle verdier

Risiko:

Vurdert konsekvens: **Liten (1)**

Kommentar: [Ingen registreringer]

Farekilde: Supercritical drying

Uønsket hendelse: Spill of acetone

Sannsynlighet for hendelsen (felles for alle konsekvensområder): **Lite sannsynlig (2)**

    Kommentar:
    [Ingen registreringer]

Konsekvensområde: Helse *Risiko:*

    Vurdert konsekvens: **Liten (1)**

        Kommentar: [Ingen registreringer]

Konsekvensområde: Materielle verdier *Risiko:*

    Vurdert konsekvens: **Liten (1)**

        Kommentar: [Ingen registreringer]

Uønsket hendelse: leak of CO2

Sannsynlighet for hendelsen (felles for alle konsekvensområder): **Svært lite sannsynlig (1)**

    Kommentar:
    [Ingen registreringer]

Konsekvensområde: Helse *Risiko:*

    Vurdert konsekvens: **Liten (1)**

        Kommentar: [Ingen registreringer]

Konsekvensområde: Materielle verdier

Vurdert konsekvens: **Liten (1)**

Kommentar: [Ingen registreringer]

Risiko:

Oversikt over besluttede risikoreduserende tiltak:

Under presenteres en oversikt over risikoreduserende tiltak som skal bidra til å reduseres sannsynlighet og/eller konsekvens for uønskede hendelser.

Detaljert oversikt over besluttede risikoreduserende tiltak med beskrivelse:

Detaljert oversikt over vurdert risiko for hver farekilde/uønsket hendelse før og etter besluttede tiltak

Appendix B

Iron and Alginate concentrations

Calculations for making iron-nitrate ($Fe(NO_3)_3$): The type of iron nitrate for this experiment was $Fe(NO_3)_3 \cdot 9\ H_2O$. It was determined to make a iron nitrate solution ($Fe(NO_3)_3$) (0.1 M) into a volumetric flask (500 mL).

The amount of mole of iron is given by the Equation B.1:

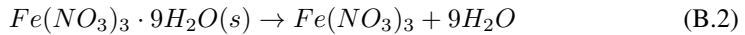$$n_{Fe(NO_3)_3} = C_{Fe(NO_3)_3} \cdot V_{solution} = 0.1M \cdot 0.500L = 0.05mole \qquad \text{(B.1)}$$

When $Fe(NO_3)_3 \cdot 9\ H_2O$ will be dissolved in water the reaction will follow reaction Equation B.2:

$$Fe(NO_3)_3 \cdot 9H_2O(s) \rightarrow Fe(NO_3)_3 + 9H_2O \qquad \text{(B.2)}$$

The stoichiometric ratio between $Fe(NO_3)_3 \cdot 9\ H_2O$ and $Fe(NO_3)_3$ are 1:1 shown from Equation B.2. The molecular weight for $Fe(NO_3)_3 \cdot 9\ H_2O$ is 403.85 g/mole. The necessary mass of $Fe(NO_3)_3 \cdot 9\ H_2O$ for 0.1 M of $Fe(NO_3)_3$ is shown from Equation B.3:

$$m_{Fe(NO_3)_3 \cdot 9H_2O} = Mm_{Fe(NO_3)_3 \cdot 9H_2O} \cdot n_{Fe(NO_3)_3 \cdot 9H_2O} = 403,85g/mole \cdot 0,05mole = 29.19g \qquad \text{(B.3)}$$

Calculations for making alginate solutions: It was determined to make 2.5, 5, 10, 15 and 20 wt% of alginate solutions. The solutions were produced from weight out the values from Tabell B.1:

Table B.1: Overview for concentrations for alginate solutions for production of catalysts.

wt%	2.5	5.0	10.0	15.0	20.0
weight of alginate [g]	0.25	0.50	1.00	1.50	2.00
volume of deionized water [mL]	9.75	9.5	9.0	8.5	8.0

Appendix C

TGA

CALCULATIONS FOR LOADING OF IRON FROM TGA RESULTS:
The loading of iron is estimated by the ratio of iron and iron(II)oxide:

$$\text{Loading of iron} = \frac{2Mm_{Fe}}{Mm_{Fe_2O_3}} \cdot \text{rest mass at } 900°C \qquad \text{(C.1)}$$

$Mm_{Fe_2O_3}$= 159.7 g/mole
Mm_{Fe}=55.85 g/mole Calculation for loading of iron for 2.5 wt% ambient dried sample is shown in Equation C.2:

$$\text{Loading of iron for 2.5 wt\% ambient dried} = \frac{2 \cdot 55.85g/mole}{159,7g/mole} \cdot 18,78\% = 13.13 \quad \text{(C.2)}$$

The calculations are accomplished for all the samples and the results are listed in Table C.1:

Table C.1: Loading of iron for the samples analyzed with TGA in air

Sample	Rest mass at 900°C (%)	Loading of iron
2.5 wt% Ambient dried	18.78	13.13
5.0 wt% Ambient dried	16.91	11.83
10 wt% Ambient dried	14.21	9.94
15 wt% Ambient dried	10.88	7.61
20 wt% Ambient dried	4.44	3.11
20 wt% Pyrolyzed 400°C 1h	16.53	12.26
20 wt% Pyrolyzed 500°C 1h	32.61	22.81
20 wt% Pyrolyzed 500°C 1h reproduced	26.85	18.78
20 wt% Pyrolyzed 600°C 1h	34.90	24.41
20 wt% Pyrolyzed 500°C 8h	39.53	27.65
20 wt% Pyrolyzed 700°C 8h	39.33	27.51

ICP-MS

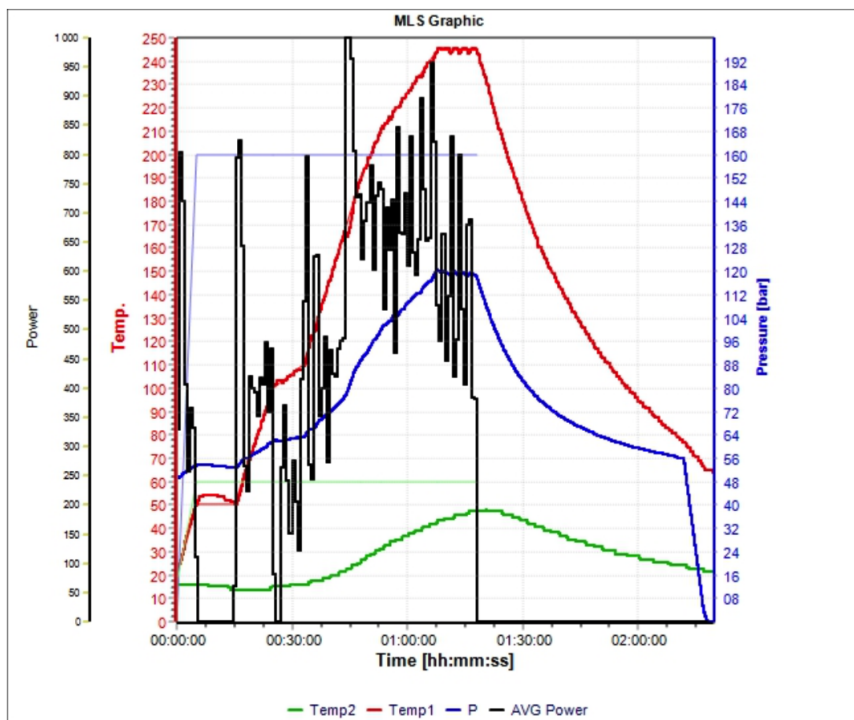Temperature profile for ICP-MS is shown in Figure D.1:

Figure D.1: Temperature profile for ICP-MS

Concentration (wt%) for Fe, Na, Al, Si, P, S, Cl and Ca for the different samples are shown in Tables D.1 and D.2:

Table D.1: Concentration for Fe, Na, Al and Si for the samples analyzed with ICP-MS

Sample	Fe (wt%)	Na (wt%)	Al (wt%)	Si (wt%)
Na alginate	0	9.28	0.001	0.006
2.5 wt% Ambient dried	12.90	0.02	0.016	0.066
5.0 wt% Ambient dried	11.29	0.02	0.016	0.054
10 wt% Ambient dried	10.64	0.02	0.010	0.040
15 wt% Ambient dried	10.19	0.06	0.010	0.025
20 wt% Ambient dried	6.0	0.21	0.009	0.019
20 wt% Pyrolyzed 400°C 1h	10.0	1.24	0.022	0.049
20 wt% Pyrolyzed 500°C 1h	27.40	0.25	0.025	0.055
20 wt% Pyrolyzed 500°C 1h reproduced	16.40	0.75	0.032	0.053
20 wt% Pyrolyzed 600°C 1h	28.36	0.38	0.017	0.046
20 wt% Pyrolyzed 500°C 8h	26.19	0.36	0.033	0.111
20 wt% Pyrolyzed 700°C 8h	26.55	0.57	0.022	0.041

Table D.2: Concentration for P, S, Cl and Ca for the samples analyzed with ICP-MS

Sample	P (wt%)	S (wt%)	Cl (wt%)	Ca (wt%)
Na alginate	0,009	0,186	0,040	0,004
2.5 wt% Ambient dried	0,015	0,061	0,043	0,006
5.0 wt% Ambient dried	0,014	0,078	0,030	0,022
10 wt% Ambient dried	0,010	0,077	-	0,003
15 wt% Ambient dried	0,009	0,054	-	0,013
20 wt% Ambient dried	0,009	0,053	-	0,003
20 wt% Pyrolyzed 400°C 1h	0,025	0,076	-	0,013
20 wt% Pyrolyzed 500°C 1h	0,026	0,180	0,039	0,010
20 wt% Pyrolyzed 500°C 1h reproduced	0,029	0,222	-	0,009
20 wt% Pyrolyzed 600°C 1h	0,029	0,270	0,042	0,011
20 wt% Pyrolyzed 500°C 8h	0,027	0,261	0,056	0,005
20 wt% Pyrolyzed 700°C 8h	0,031	0,230	0,059	0,006

Appendix E

Theoretical Fe loading

Calculations for the theoretical loading of iron at the different concentrations of alginate. Iron will ion exchange with sodium.

One mole of iron will react with two moles of alginate. The sodium will be washed away.

Table E.1: Chemical data for sodium, iron and alginate. Values found from (1).

$Mm_{Na-alginate}$ [g/mole]	216.1
Mm_{Na} [g/mole]	22.99
$Mm_{alginate}$ [g/mole]	193.1
Mm_{Fe} [g/mole]	55.85
n_{Fe} [mole]	0.005
$Mm_{Fe+2Alginate}$ [g/mole]	442.07

$$\text{Loading of Fe} = \frac{Mm_{Fe}}{Mm_{Fe+2Alginate}} = \frac{55.85 g/mole}{442.07 g/mole} \cdot 100\% = 12.6\% \qquad (E.1)$$

The amount of mole of alginate is given by the Equation E.2:

$$n_{Na-alginate} = \frac{m_{Na-alginate}}{Mm_{Na-alginate}} \qquad (E.2)$$

Calculation for 2.5 wt% alginate is calculated from Equation E.2 and shown in Equation E.3:

$$n_{alginate}2.5wt\% = \frac{0,25g}{216,1g/mole} = 1,16 \cdot 10^{-3}mole \qquad (E.3)$$

Same calculation as Equation E.2 are accomplished for all the different concentrations of alginate and listed in Table E.2: Calculation of iron and alginate is shown in E.4:

$$\frac{n_{Fe}}{n_{alginate}} \qquad (E.4)$$

Table E.2: Amount of alginate and ratio Fe/alginate for the different concentrations for alginate

Sample	$m_{alginate}$ [g]	$n_{alginate}$ [mole]	$n_{Fe}/n_{alginate}$
2.5 wt% Ambient dried	0,25	$1,16 \cdot 10^{-3}$	4,32
5.0 wt% Ambient dried	0,50	$2,31 \cdot 10^{-3}$	2,16
10 wt% Ambient dried	1,00	$4,63 \cdot 10^{-3}$	1,08
15 wt% Ambient dried	1,50	$6,94 \cdot 10^{-3}$	0,72
20 wt% Ambient dried	2,00	$9,25 \cdot 10^{-3}$	0,54

The Fe alginate ratio are always over 0,5 so alginate will always be the limiting reactants.

Appendix F

Calculations for HPFT

The Gas Hour Space Velocity (GHSV) for the catalysts are calculated from Equation 2.12
The catalysts tested in the High Pressure FT:

- 20 wt% Pyrolyzed 400°C 1h

- 20 wt% Pyrolyzed 500°C 1h

- 20 wt% Pyrolyzed 500°C 1h reproduced

- 20 wt% Pyrolyzed 600°C 1h

- 20 wt% Pyrolyzed 700°C 8h

- Reference Catalyst

Table F.1: Iron loading, mass of catalyst, CO conversion, Selectivity of CO_2 and Flow of CO for the catalysts tested at HPFT. (340°C, 20 bar)

Sample	Iron loading [%]	$m_{catalyst}$ [g]	CO Conversion [%]	S_{CO_2} [%]	F_{CO} [mL/min]
20 wt% Pyrolyzed 400°C 1h	10.0	0.25	26.4	41.2	$0.485 \cdot F_{250ml/min}$
20 wt% Pyrolyzed 500°C 1h	27.4	0.50	67.0	45.7	$0.485 \cdot F_{598.6ml/min}$
20 wt% Pyrolyzed 500°C 1h reproduced	16.4	0.25	65.0	45.1	$0.485 \cdot F_{250ml/min}$
20 wt% Pyrolyzed 600°C 1h	28.4	0.25	64.0	46.2	$0.485 \cdot F_{250ml/min}$
20 wt% Pyrolyzed 700°C 8h	26.6	0.25	65.0	45.5	$0.485 \cdot F_{250ml/min}$
Reference Catalyst	92.0	0.25	42.0	47.3	$0.485 \cdot F_{250ml/min}$

*S_{CO_2} values at the conversions for the catalyst. 20 wt% Pyrolyzed 500°C 1h was tested at the different flows 269,4, 299,3 and 598,6 mL/min. The catalyst mass for 20 wt%

Pyrolyzed 500°C 1h was 0,5 g. GHSVs for the flows for 20 wt% Pyrolyzed 500°C 1h are shown in Equation F.1 - F.3:

$$GHSV_{0,5g,269,4ml/min} = \frac{\frac{269,4mL/min}{60s/min}}{0,5g \cdot \frac{1}{3600s/h}} = 32328 \tag{F.1}$$

$$GHSV_{0,5g,299,3ml/min} = \frac{\frac{299,3mL/min}{60s/min}}{0,5g \cdot \frac{1}{3600s/h}} = 35916 \tag{F.2}$$

$$GHSV_{0,5g,598,6ml/min} = \frac{\frac{598,6mL/min}{60s/min}}{0,5g \cdot \frac{0,25g}{3600s/h}} = 71832 \tag{F.3}$$

GHSV when the mass was 0,25g and the flow was 250 mL/min

$$GHSV_{0,25g,250ml/min} = \frac{\frac{250mL/min}{60s/min}}{0,25g \cdot \frac{1}{3600s/h}} = 60000 \tag{F.4}$$

$$GHSV_{0,25g,125ml/min} = \frac{\frac{125mL/min}{60s/min}}{0,25g \cdot \frac{1}{3600s/h}} = 30000 \tag{F.5}$$

Iron Time Yield (FTY) for the catalysts are calculated from Equation F. The molar volume V_m is 24.465 L/mole (1) 1 atm and 25 °C. This conditions molar volume are based on the inlet conditions for the syngas (1 atm and 25 °C). The calculations for FTY for the catalysts are shown in Equation F.6- F.11:

$$FTY = X_{CO} \cdot F_{CO}\left(\frac{1 - S_{CO_2}}{V_m \cdot 60 \cdot m_{cat} \cdot \frac{X_m}{100}}\right)$$

$$FTY_{400°C1h} = 0.264 \cdot 0.485 \cdot 250 \cdot 10^{-3} \cdot \frac{(1 - 0.412)}{24.465 \cdot 60 \cdot 0.25 \cdot 0.1} = 5.1 \cdot 10^{-4} molCO/g_{Fe}s \tag{F.6}$$

$$FTY_{500°Ch} = 0.6692 \cdot 0.485 \cdot 598.659 \cdot 10^{-3} \frac{(1 - 0.45731)}{24.465 \cdot 60 \cdot 0.25 \cdot 0.274} = 5.2 \cdot 10^{-4} molCO/g_{Fe}s \tag{F.7}$$

$$FTY_{500°C1hreproduced} = 0.6479 \cdot 0.485 \cdot 250 \cdot 10^{-3} \frac{(1 - 0.45109}{24.465 \cdot 60 \cdot 0.25 \cdot 0.164} = 7.2 \cdot 10^{-4} molCO/g_{Fe}s \tag{F.8}$$

$$FTY_{600°C1h} = 0.6349 \cdot 0.485 \cdot 250 \cdot 10^{-3} \frac{(1 - 0.46209}{24.465 \cdot 60 \cdot 0.25 \cdot 0.2836} = 4.0 \cdot 10^{-4} molCO/g_{Fe}s \tag{F.9}$$

$$FTY_{700^\circ C8h} = 0.6538 \cdot 0.485 \cdot 250 \cdot 10^{-3} \frac{(1 - 0.45525}{24.465 \cdot 60 \cdot 0.25 \cdot 0.266} = 7.2 \cdot 10^{-4} molCO/g_{Fe}s$$
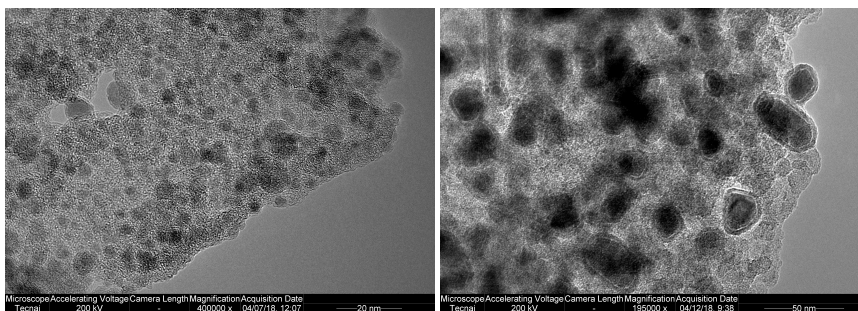
<div align="right">(F.10)</div>

$$FTY_{Referencecatalyst} = 0.4148 \cdot 0.485 \cdot 250 \cdot 10^{-3} \frac{(1 - 0.473028}{24.465 \cdot 60 \cdot 0.25 \cdot 0.92} = 7.9 \cdot 10^{-5} molCO/g_{Fe}s$$

<div align="right">(F.11)</div>

Appendix G

TEM Pictures of High Pressure FT

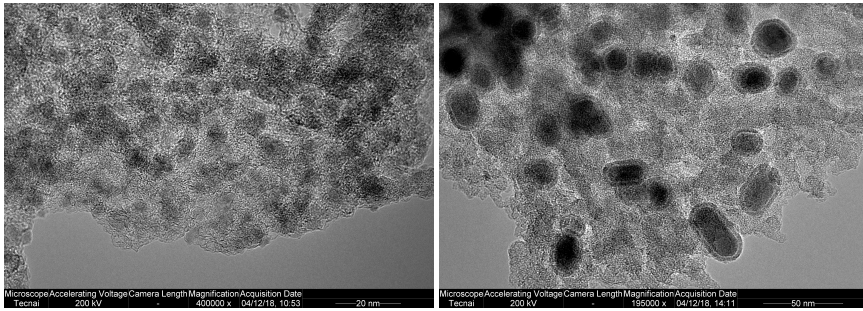The samples analyzed with TEM before and after testing in the HPFT were:

- 20 wt% Pyrolyzed 500°C 1h

- 20 wt% Pyrolyzed 600°C 1h

- 20 wt% Pyrolyzed 700°C 8h

(a) TEM picture of
600°C 1h
before tested
in FT. TEM picture
taken in China

(b) TEM picture of
600°C 1h
after testing
in FT. TEM picture
taken in China

Figure G.1: 600°C 1h before and after testing in HPFT taken in China

(a) TEM picture of
700°C 8h
before tested
in FT. TEM picture
taken in China

(b) TEM picture of
700°C 8h
after testing
in FT. TEM picture
taken in China

Figure G.2: 700°C 8h before and after testing in HPFT taken in China